Featured in Physics

Dense and Hot QCD at Strong Coupling

Tuna Demircik[1,*], Christian Ecker[2,†] and Matti Järvinen[1,3,‡]

[1]*Asia Pacific Center for Theoretical Physics, Pohang, 37673, Korea*
[2]*Institut für Theoretische Physik, Goethe Universität,*
Max-von-Laue-Straße 1, 60438 Frankfurt am Main, Germany
[3]*Department of Physics, Pohang University of Science and Technology, Pohang, 37673, Korea*

We present a novel framework for the equation of state of dense and hot quantum chromodynamics (QCD), which focuses on the region of the phase diagram relevant for neutron star mergers and core-collapse supernovae. The model combines predictions from the gauge/gravity duality with input from lattice field theory, QCD perturbation theory, chiral effective theory, and statistical modeling. It is therefore, by construction, in good agreement with theoretical constraints both at low and high densities and temperatures. The main ingredients of our setup are the nonperturbative V-QCD model based on the gauge/gravity duality, a van der Waals model for nucleon liquid, and the DD2 version of the Hempel-Schaffner-Bielich statistical model of nuclear matter. By consistently combining these models, we also obtain a description for the nuclear to quark matter phase transition and its critical end point. The parameter dependence of the model is represented by three (soft, intermediate, and stiff) variants of the equation of state, all of which agree with observational constraints from neutron stars and their mergers. We discuss resulting constraints for the equation of state, predictions for neutron stars, and the location of the critical point.

Subject Areas: Astrophysics, Nuclear Physics
Particles and Fields

I. INTRODUCTION

Solving QCD at intermediate density and temperature is a long-standing open problem. Recent and upcoming developments in relativistic heavy ion collision experiments and astrophysical observations of compact stars as well as their mergers urgently demand progress in the theoretic modeling of QCD at few times nuclear saturation density $n_s = 0.16$ fm^{-3} and temperatures up to around 100 MeV. First-principles approaches such as lattice QCD and perturbation theory are not applicable in the relevant regime, and effective field theory only works up to densities around the nuclear saturation density. Despite recent progress in finite-temperature chiral effective theory (CET) computations at high loop order [1], typical densities and temperatures such as estimated by realistic binary neutron star merger simulations [2–7] remain currently out of reach.

A central quantity that is absolutely crucial in the modeling of compact stars is the equation of state (EOS). Because of the aforementioned lack of first-principles results, the QCD EOS at intermediate densities currently has large uncertainties at zero temperature, and even less is known about the temperature dependence. These uncertainties motivate us to formulate a novel framework, which combines predictions from various different approaches in different temperature and density regions of the QCD phase diagram where they are expected to work best. The main idea is to use gauge/gravity duality to model the physics at large and intermediate densities, and combine this with effective theory at low densities. This combination allows us to establish a unified description of QCD matter for a wide range of densities and temperatures including, but not limited to, the ranges relevant for core-collapse supernovae and neutron star mergers.

The QCD phase diagram is conjectured to include a critical point where the nuclear to quark matter (QM) transition ends. Ongoing experiments at RHIC (the beam energy scan) already probe the region of the phase diagram where the critical point may lie [8]. Future experiments at FAIR [9,10] and NICA [11] will provide more detailed information about this region, and will reach substantially higher densities, i.e., densities well above the nuclear saturation density. Consequently, it is timely to improve

*tuna.demircik@apctp.org
†ecker@itp.uni-frankfurt.de
‡matti.jarvinen@apctp.org

theoretical predictions for the location of the critical point and the EOS in its vicinity. Our approach leads to EOS which are in good agreement, among other things, with lattice data at small density as well as with *ab initio* calculations and observational data from neutron star measurements at finite density and small temperature. Therefore we are able to obtain controlled interpolations of the EOS to the theoretically challenging region of intermediate densities ($n_s \lesssim n_b \lesssim 10 n_s$) and low temperatures ($T \lesssim 150$ MeV), and sound estimates for the location of the critical point.

The model, which we construct in this article, is a thermodynamically consistent combination of three main approaches: the holographic V-QCD model [12,13], an adjusted van der Waals (vdW) model of nuclear matter [14], and the nuclear theory model Hempel-Schaffner-Bielich (HS) EOS [15] with DD2 relativistic mean-field (RMF) theory interactions [16]. We also use the Akmal-Pandharipande-Ravenhall (APR) model [17] of cold nuclear matter and a meson gas model near the QCD crossover region (see Fig. 1), but they play a smaller role in the final EOS. The reason we use the APR model rather than HS (DD2) for cold nuclear matter near the saturation density is because if we used HS(DD2) only, the resulting EOS would be so stiff that it would be in conflict with the LIGO-Virgo measurement of the tidal deformability for GW170817.

We use V-QCD [12,13], which is a nonperturbative model for QCD that is based on the gauge/gravity duality, at intermediate and high densities, i.e., densities above the nuclear saturation density. This model allows us to describe both the nuclear and quark matter phases and therefore the phase transition in a single framework. It has been shown [18,19] to lead to a feasible EOS for cold QCD matter which is in good agreement with all available data.

Its extension to finite temperature is, however, problematic due to a generic limitation in gauge/gravity duality that the EOS in confined phases, including the nuclear matter phase, is independent of temperature and therefore not fully realistic. In the absence of other reliable ways to estimate the temperature dependence of the EOS for dense nuclear matter, we use essentially the simplest approach: a

van der Waals type model of nuclear matter, i.e., a gas of nucleons and electrons with excluded volume (EV) corrections and an effective potential. The effective potential is tailored for the model to agree with V-QCD at zero temperature, and therefore the van der Waals model gives an extrapolation of the V-QCD nuclear matter result to finite temperatures. The third and final main constituent of the model is the nuclear theory model at low densities (below and around nuclear saturation density). In this article, we use the HS(DD2) model.

Figure 1 shows a sketch of the building blocks and the resulting phase structure [20] of our model and their dependence on temperature and density, which is the main topic of this article. This dependence is completed by the dependence on the charge fraction Y_q, i.e., allowing deviation from β equilibrium, while imposing charge neutrality, which is required for realistic simulations of neutron star mergers and core-collapse supernovae. For this dependence we use the prediction of the HS(DD2) model in the nuclear matter (NM) phase and a simple model, arising from the pressure of free electrons, in the QM phase whose construction we discuss in Sec. III. D. We provide three tabulated variants of the density, temperature, and charge-fraction-dependent EOS of this article in the CompOSE database [21,22].

Naturally, constructing such a complicated model, which covers regions of the phase diagram where direct theoretical input from QCD is lacking, requires use of approximations and simplifications. In particular the use of the vdW model for the temperature dependence does not reflect the complicated dynamics of QCD in the regime of dense nuclear matter. However, in the absence of reliable first-principles computations of the temperature dependence, using simple models might be the most reasonable option. Similar comments apply to the dependence on charge fraction, which we adopt from the HS(DD2) model using mean-field theory in this region, and from an even simpler model in the quark matter phase. We also remark that the region near the critical point in Fig. 1 is modeled through a combination of three different models, which suggests that only rough features of the EOS can be reliable.

The final model depends on a large number of parameters arising from the various approaches that it uses, and from choices on how they are merged. While the parameter space is subject to severe observational and theoretical constraints, it is important to analyze the remaining dependence on the parameters. Because of the complexity of the model, we limit the study of this article to the largest uncertainty arising from the parameter dependence on the holographic V-QCD model. We remark, however, that one of the main motivations of the combined framework of this article is the overall reduced parameter dependence of the final predictions. While we do not carry out a complete analysis of this dependence here, it has been studied in detail for the zero temperature reduction of the model. Indeed, our hybrid method of using the most suitable model
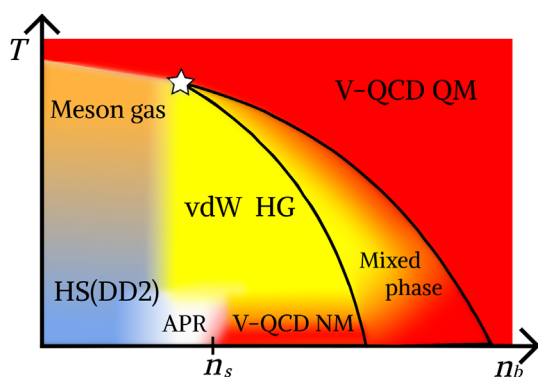

FIG. 1.   A schematic diagram that shows the construction for the temperature dependence in the model. See text for details.

in each region of the phase diagram together with imposing constraints from neutron star observations leads to significantly more constrained predictions and less arbitrary final results than generic (polytropic) EOS models for cold QCD matter [19,23].

Finally, let us comment on how the model of this article is related to other recent research on the EOS of QCD. The cold versions of the model, i.e., hybrid EOS using V-QCD for dense nuclear and quark matter at zero temperature and at β equilibrium, and various models for the low density nuclear matter, were established and studied in Refs. [18,19].

They have been applied in simulations of binary neutron star mergers [18] and the study of rapidly rotating isolated stars [24]. A related work [25] combined the HS(DD2) model and two other general purpose models for the EOS directly with the quark matter EOS from V-QCD, producing models for the EOS with dependence on temperature and charge fraction outside β equilibrium. In the current article, we extend this work, among other things, by including the description of nuclear matter from gauge/gravity duality and its temperature dependence, which is our main focus, and also allows a consistent description of the mixed nuclear-quark matter phase. Another framework for the transition where nuclear and quark matter are described on an equal footing is Ref. [26], where cluster expansion was used (see also Ref. [27]). A recent article [28] considered models in the van der Waals class for hot and dense nuclear matter. Their focus was matching the predictions of chiral effective theory with the vdW models at low density, and to use the vdW models to extend the results to higher densities and temperatures, whereas in the current work we use the vdW model to extrapolate the holographic cold hybrid EOS (which is feasible for all densities) to finite temperatures.

There are several earlier studies of dense QCD matter which combine equations of state from different models. In models of nuclear matter, it is typical to use different approaches for densities above and below the nuclear saturation density, and the approach of Ref. [15], which we also use in part in our construction, is an example of this. When including quark matter it is likewise typical to use combinations of models: examples of such approaches are Refs. [29,30], which combine different approaches for dense nuclear matter with the Nambu-Jona-Lasinio model for quark matter at finite temperature, and Ref. [31], which uses a similar approach but includes color superconducting and color-flavor locked phases. Examples of other hybrid approaches are Refs. [32–34]. Available general purpose EOS, which similarly to our construction include both nuclear and quark matter phases with dependence on temperature and charge fraction, include two methods. The first method uses the Shen-Toki-Oyamatsu-Sumiyoshi EOS [35,36] for nuclear matter with the MIT bag model for quark matter [37–40]. The second method uses the HS

(DD2) with a relativistic mean-field approach for quark matter [41,42]. We compare our predictions to two models in this latter class, as well as to well-established nuclear theory models without quark matter, in Appendix D. In addition, there is a recently constructed general purpose EOS [43] which uses an extended bag model with the Bombaci-Logoteta EOS [44]. See also the reviews of EOS for supernovae and compact stars [45,46].

The article is organized as follows. In Sec. II, we review the various building blocks of our approach. In Sec. III, we show how the results for the EOS from these building blocks can be combined into a single thermodynamically consistent EOS. In Sec. IV, we analyze the EOS, predictions for the critical point, and predictions for nonrotating neutron stars. Our conclusions and future directions are given in Sec. V. We additionally provide technical details on the construction of our EOS (Appendix A), compare the vdW model to the nuclear matter part of V-QCD (Appendix B), explain how we determine our predictions for the QCD critical point (Appendix C), and carry out a detailed comparison of our EOS to earlier work (Appendix D).

Throughout this article we use Planck units where $c = \hbar = k_B = 1$.

II. BUILDING BLOCKS OF THE MODEL

We start the discussion of our model by briefly reviewing the various building blocks of the model.

A. Holographic V-QCD

A central ingredient in our setup is the use of the gauge/gravity duality. It maps, in general, strongly coupled four-dimensional field theory to classical five-dimensional gravity. Therefore, challenging questions on the field theory side can be solved by carrying out a simple classical analysis on the dual gravity side. In this work we use the V-QCD model in regions which do not admit a weakly coupled description in terms of quarks, gluons, or hadrons. V-QCD is an effective gauge-gravity model in the sense that it contains a relatively large number of parameters that are tuned to match with QCD data from experiments, lattice analysis, and perturbation theory. This is particularly useful in the context of hot and dense QCD as there are plenty of lattice data available at low density, and gauge-gravity models can be used to extrapolate these data to higher densities at which first-principles methods are not available [47–50]. Similar approaches have also been implemented by using field theory, e.g., within the Polyakov-loop extended Nambu–Jona-Lasinio model [51] and the Polyakov-quark-meson model of Refs. [52,53]. Applying these ideas to V-QCD has been shown to lead to feasible and well-constrained EOS for both dense quark [54] and nuclear matter [13,18,19]. This means the model is also able to describe the nuclear to quark matter phase transition in a single framework.

Let us then explain briefly how V-QCD is constructed. We discuss here only the main features of the model and refer the reader to Ref. [55] for a complete review with precise definitions. The model contains both a gluon sector, given by the improved holographic QCD model (five-dimensional dilaton gravity) [56,57], and a flavor sector arising through a pair of space filling flavor branes [58,59]. The flavors are dynamical: full backreaction of the branes to the geometry is included formally by working in the Veneziano limit [60,61] where both the number of colors N_c and flavors N_f is large but their ratio is $\mathcal{O}(1)$ [12]. Note that while the theory in the Veneziano limit is the starting point, in the end one switches to a bottom-up approach, where the contact of the holographic model to any specific field theory is lost. As we stressed above, the final mode should be seen as an effective model that is fitted to QCD at physical values of N_c and N_f.

A basic feature of the gauge/gravity duality is that various phases in the field theory map to different geometries in the five-dimensional gravity theory. In the case of V-QCD, there are two possible geometries. The first is a horizonless geometry ending at a "good" kind of infrared singularity [62] and the second is "planar" black hole solution. The black holes can be charged, which is interpreted as a nonzero baryon number arising from deconfined quark matter [63,64]. The gravitational solution includes a scalar condensate in the confined phase, which is dual to the chiral condensate of QCD therefore implementing chiral symmetry breaking [12,58,59]. These geometries are therefore dual to a chirally broken confined hadron gas (HG) phase and a chirally symmetric deconfined quark-gluon plasma phase, respectively. For the plain confined geometry, the thermodynamics is trivial in the sense that, for example, the pressure is independent of temperature and chemical potential; we will use other methods in this region as we discuss below. For the deconfined phase, the temperature and entropy density are calculated through black hole thermodynamics [63–66]. Apart from hadron gas and quark matter, we consider nuclear matter by employing the approach of Ref. [13]. The nuclear matter phase is obtained in an approximation that is based on a homogeneous five-dimensional bulk field in the confined horizonless geometry. The five-dimensional action of the model is then obtained schematically as a sum of three terms:

$$S_{\text{V-QCD}} = S_g + S_f + S_{\text{NM}}, \qquad (1)$$

where the first one (S_g) is the action for improved holographic QCD, i.e., the gluon sector of the model, the second one (S_f) is the flavor brane action important in the quark-gluon plasma and quark matter phases, and (S_{NM}) is the action for homogeneous nuclear matter derived in Ref. [13].

We do not present the details of the actions here, but as we pointed out above, they contain a relatively high number of parameters that need to be tuned to match the model with QCD data. First, the model must agree with known features of QCD such as asymptotic freedom, confinement, linear glueball and meson trajectories, and chiral symmetry breaking. Second, those parameters that are left free after considering such qualitative constraints are fitted to lattice data for thermodynamics of QCD [54,67]. Specifically, we use lattice data for the equation of state of large-N_c pure Yang-Mills [68] and data for $N_c = 3$ QCD with $N_f = 2 + 1$ flavors at physical quark masses [69,70] at small baryon number density. Interestingly, the fit is stiff in the sense that the dependence of the various model parameters is mild, but despite this a fit of high quality is possible with all the parameter values remaining in a natural range. At the moment, the fit uses flavor-independent quarks with zero mass. See the review [55] for a detailed discussion of this fit and the comparison of the model with QCD in general.

After determining the model parameters, V-QCD has a natural phase diagram that includes both nuclear and quark matter [13,55]. The EOS for quark matter agrees with QCD lattice data at zero density and finite temperature, with perturbative QCD for high values of the baryon number chemical potential and/or temperature, and with constraints for the EOS of cold quark matter EOS at low density [25,54]. Note, however, that we have not included electrons or photons, and as the quark flavors are identical, there is no dependence on charge fraction. For the full model EOS in the quark matter phase, we also need to model these features, i.e., the electron pressure and the dependence on charge fraction. We discuss this in Sec. II.

In the nuclear matter phase, the model is feasible at zero temperature and can be used to construct phenomenologically viable EOS for cold QCD matter as was done in Refs. [18,19,23]. However, there is an issue with the extension to finite temperature: the thermodynamics is temperature independent in the confined phases, as we pointed out above. This is a rather generic feature of gauge/gravity duality and arises due to taking the limit of large N_c: the pressure of confined color singlet hadron states, which are the constituents of the confined matter, is suppressed by $1/N_c^2$ with respect to the pressure of the deconfined matter [71]. Because of this issue, the thermodynamics in the confined "hadron gas" phase without nuclear matter is trivial, i.e., that of empty space. But also in the nuclear matter phase, the temperature dependence is absent. While this result may be a rather good zeroth-order approximation, it prevents us from building a fully realistic EOS directly based on V-QCD. In order to cure this issue, we use a vdW model instead for the temperature dependence, which we discuss next.

B. van der Waals hadron gas model

The vdW model consists of a bosonic and a fermionic sector. The ideal gas pressure of the whole system is

$$p_{\text{id}}(T, \{\mu_k\}) = \sum_i p_{\text{FD}}^{(i)}(T, \mu_i, m_i)$$
$$+ \sum_j p_{\text{BE}}^{(j)}(T, m_j) + p_\gamma(T). \quad (2)$$

The first term $p_{\text{FD}}^{(i)}$ is the fermionic contribution that describes nucleons, antinucleons, electrons, and positrons denoted by the index $i \in \{n, \bar{n}, p, \bar{p}, e, \bar{e}\}$. The bosonic sector is given by the last two terms, where $p_{\text{BE}}^{(j)}$ and p_γ are the contributions of mesons and photons, respectively. We include all mesons with $m_j \leq 1$ GeV from the particle data group listings [72]. The photon contribution $p_\gamma(T) = \pi^2 T^4/45$ is simply that of a blackbody photon gas. The pressure of a relativistic ideal Fermi (Bose) gas is given by

$$p_{\text{FD or BE}}^{(k)}(T, \mu_k, m_k) = \frac{g_k}{6\pi^2} \int_0^\infty \frac{p^4}{E_k} \frac{dp}{e^{(E_k - \mu_k)/T} \pm 1}, \quad (3)$$

wherein the index k denotes the fermion (boson) species with relativistic dispersion relation $E_k = \sqrt{p^2 + m_k^2}$, $+(-)$ is for fermions (bosons), and g_k is the spin degeneracy factor. We also note that different fermion and antifermion species have different chemical potentials while $\mu_k = 0$ for the bosonic sector.

It is well known that the ideal hadron gas (IHG) picture has vital shortcomings. Perhaps most importantly, it fails in describing the ground state of NM, viz., saturation of NM at $T = 0$ and $n = n_s$. The reason for this shortcoming is the fact that the IHG does not capture repulsive and attractive vdW interactions of nucleons. Repulsive vdW interactions are often implemented via excluded volume corrections describing a hard-core repulsion of nucleons. The thermodynamically consistent formulation of an IHG with EV correction was developed in Ref. [73] (see also Ref. [74]). A more natural picture of vdW interactions that realizes both the short-range repulsive and the intermediate-range attractive interactions was formulated in Refs. [75,76] (see Ref. [14] for a more complete list of references). The parameters of the vdW interactions are typically fixed by requiring consistency with the saturation density n_s and binding energy per nucleon of the ground state $\epsilon_B/n_b = -16$ MeV [77,78].

In our construction, we follow a different strategy and use holography as guidance to model vdW interactions. In the rest of this section, we present our implementation of repulsive vdW interactions via EV corrections by employing the formulation in Ref. [73]. Attractive vdW interactions are incorporated by a direct matching to the cold V-QCD hybrid EOS at β equilibrium described in Sec. III B.

The excluded volume corrected pressure is defined implicitly by introducing a shifted chemical potential $\tilde{\mu}_i$:

$$p_{\text{ex}}(T, \{\mu_k\}) = p_{\text{id}}(T, \{\tilde{\mu}_k\}), \quad (4)$$

$$\tilde{\mu}_i = \mu_i - v_i p_{\text{ex}}(T, \{\mu_k\}). \quad (5)$$

We choose $v_p = v_{\bar{p}} = v_n = v_{\bar{n}} = v_0$, $v_e = v_{\bar{e}} = 0$ and set $v_0 = 0.56$ fm^3. The choice of v_0 is motivated by comparison with V-QCD EOS at $T = 0$. More details about our choice and a comparison of different values for v_0 are given in Appendix B.

The number density is found by differentiating Eq. (4):

$$n_{\text{ex}}^{(i)}(T, \{\mu_k\}) = \frac{\partial p_{\text{ex}}(T, \{\mu_k\})}{\partial \mu_i}$$
$$= \frac{n_{\text{id}}^{(i)}(T, \{\tilde{\mu}_k\})}{1 + v_0 \sum_l n_{\text{id}}^{(l)}(T, \{\tilde{\mu}_k\})}, \quad (6)$$

where $n_{\text{id}}^{(i)} = \partial p_{\text{id}}(T, \{\tilde{\mu}_k\})/\partial \mu_i$ and i denotes the fermion species, while the index l runs over only nucleons and antinucleons. At this point, we fix the chemical potentials of antifermions as $\mu_{\bar{i}} = -\mu_i$. The total number density for each fermion species is then given by the difference between the corresponding particle and antiparticle number densities:

$$\tilde{n}_{\text{ex}}^{(i)}(T, \{\tilde{\mu}_k\}) = n_{\text{ex}}^{(i)}(T, \{\tilde{\mu}_k\}) - n_{\text{ex}}^{(\bar{i})}(T, \{\tilde{\mu}_k\}), \quad (7)$$

where $i \in \{p, n, e\}$. Requiring charge neutrality in addition,

$$\tilde{n}_{\text{ex}}^{(e)}(T, \{\mu_k\}) = \tilde{n}_{\text{ex}}^{(p)}(T, \{\tilde{\mu}_k\}), \quad (8)$$

leaves only two free chemical potentials which we choose to be μ_p and μ_n. By using Eqs. (6) and (7), the definitions for the baryon number density n_b, the charge fractions Y_q, and charge neutrality condition are obtained as

$$n_b(T, \mu_p, \mu_n) = \tilde{n}_{\text{ex}}^{(p)}(T, \mu_p, \mu_n) + \tilde{n}_{\text{ex}}^{(n)}(T, \mu_p, \mu_n), \quad (9)$$

$$Y_q(T, \mu_p, \mu_n) = \tilde{n}_{\text{ex}}^{(p)}(T, \mu_p, \mu_n)/n_b(T, \mu_p, \mu_n). \quad (10)$$

For future convenience, we conclude this section by giving the definition of the free energy, which is the natural thermodynamic potential in the canonical ensemble:

$$f_{\text{ex}}(T, n_b, Y_q) = \sum_i n_{\text{ex}}^{(i)} \mu_i(T, n_b, Y_q) - p_{\text{ex}}(T, n_b, Y_q), \quad (11)$$

where the thermodynamics is expressed in terms of variables n_b and Y_q instead of μ_p and μ_n.

C. HS(DD2) model

HS(DD2) is a commonly used EOS that was originally developed to simulate core collapse of supernovae [15,16]. It provides reliable modeling of NM below and around the saturation density, with a consistent description for the transition from nonuniform to uniform nuclear matter.

HS(DD2) consists of two different sectors. The first sector models light and heavy nuclear clusters in nuclear statistical equilibrium with EV correction. The second sector describes unbound nucleons in relativistic mean-field theory. HS(DD2) includes all possible light nuclei (e.g., deuterium, tritium, etc.) in addition to α particles and heavy nuclei up to mass number $A \sim 330$.

The RMF approach is used to model interactions of unbound nucleons with the exchange of σ, ω, and ρ mesons. At low densities, the interactions become negligible and the system reduces to an ideal Fermi-Dirac gas of nucleons. Photons are added separately as a free Bose gas and the Wigner-Seitz approximation is employed for the Coulomb interaction between electrons and nuclei. EV effects are implemented in a way to treat unbound nucleons and nuclei in a different manner: while the volume of all baryons is excluded for nuclei, unbound nucleons only feel the volume of nuclei since the interaction among them is already modeled by the RMF model.

The parameters of the RMF model are the masses of the nucleons and the mesons, and the coupling constants. In HS(DD2), the so-called TMA parameter set is used [79]. For the masses of nuclei, the experimental data [80] are used when they are available, otherwise the data are taken from nuclear calculations [81].

By construction, HS(DD2) is a thermodynamically consistent model for both nonuniform matter of light and heavy clusters within the gas of unbound nucleons at low density, uniform matter described by the RMF model above densities higher than n_s, and the transition between them. The resulting EOS are provided in three-dimensional (T, n_b, Y_q) tabular form covering a wide range. The EOS tables are publicly available on the CompOSE database [21,22]. Different variants of the model were constructed by using different sets of RMF parameters [82,83].

III. COMBINING THE BUILDING BLOCKS

In this section we discuss in detail how the various building blocks of the model are combined into a unified model (see Fig. 1).

A. Construction of the cold EOS

We start from the construction of the nuclear matter EOS at zero temperature, which mostly follows Refs. [18,19]. That is, we first construct cold hybrid EOS by combining the predictions of V-QCD with nuclear theory models at β equilibrium.

Our prescription for dense nuclear matter in the V-QCD model is based on a homogeneous bulk field in the dual gravity model, which is natural for densities well above n_s. At such high densities the average distance between neighboring nucleons is comparable to or smaller than their diameters, so that their wave functions overlap, and approximating the system as homogeneous matter is expected to work. However, this is not the case at densities below n_s, wherein homogeneous approximations will break down. This is not a problem, since in this region traditional NM models have proven to be reliable and feasible. In this sense traditional NM models and homogeneous NM in V-QCD complement each other. In Refs. [18,19], this idea was implemented to construct hybrid EOS: low density EOS from various traditional nuclear theory models were combined with the high density V-QCD NM EOS, matching them continuously at an intermediate density around $1.5n_s$–$2n_s$.

A potential weakness of the construction of Refs. [18,19] is that the matching point between the low and high density models introduces, in effect, a second-order phase transition, where, for example, the speed of sound is discontinuous. Since this matching within a single phase is not physically motivated, but only a technical necessity in our construction, it should not give rise to a sudden change in the material properties as would be the case for discontinuous sound speed. In order to smooth it out, we consider an improved matching setup with two separate matching densities in the same region of densities slightly above the saturation density. The EOS in the intermediate region between the two matching densities is chosen to have a speed of sound which is linear in the baryon number density, whereas the low and high density regions are treated as before. The slope of the speed of sound in the intermediate region is determined by requiring continuity of the speed of sound, i.e., third-order phase transitions at both the transition densities. See Appendix A 1 for details. The resulting EOS (free energy as a function of baryon number density) is denoted below as $f_{\text{cold}}(n_b)$.

In this work, we use three variants of hybrid EOS for nuclear matter at zero temperature. We select the Akmal-Pandharipande-Ravenhall model [84] for the low density regime and three variants of V-QCD at high density: these variants are defined by the data fits 5b, 7a, and 8b of Refs. [19,54]. These choices represent the leftover parameter dependence of V-QCD after the comparison with lattice data and taking into account observational constraints. If we used the approach of Refs. [18,19] with a single transition density $1.6n_s$ the hybrids with these three choices would be exactly the soft, intermediate, and stiff variants of the V-QCD (APR) EOS published in the CompOSE database [85–87]. Here the stiffness refers to a property of dense nuclear matter: the stiff EOS reaches a noticeably higher speed of sound than the soft one. In the improved approach of this article, we choose the two

transition densities to be $1.4n_s$ and $1.8n_s$. That is, the choices of the cold nuclear matter EOS in this article are practically the same as the published V-QCD (APR) variants, but the kink (say, in pressure as a function of density) at the transition density has been smoothed out.

B. Matching the vdW HG model with holography

We now discuss how the EOS for cold nuclear matter is extrapolated to finite temperatures, and also outside β equilibrium. As pointed out above, we use the vdW HG model for the temperature dependence in the dense nuclear matter phase. This approach is motivated by the fact that, for an appropriate choice of the excluded volume v_0, the EOS of the vdW model and the nuclear matter of the V-QCD model are relatively close (see Appendix B). Therefore, adding only a small, mostly attractive potential is required to match the vdW model with the cold hybrid EOS. Moreover, we add the dependence on the charge fraction outside β equilibrium by using the HS(DD2) model. In principle, one could use the vdW model also for the charge fraction. The vdW model is, however, too simple to satisfy the experimental constraints for nuclear matter below and around saturation density. In particular, the symmetry energy is too low—this is known to happen for a free gas, and excluded volume effects alone are not sufficient to improve the result [88]. We could in principle use the vdW model at higher densities, where experimental constraints do not apply, but for simplicity we adopt the Y_q dependence from HS(DD2) everywhere in the nuclear matter regime.

The above adjustments are taken into account by redefining the free energy of the dense NM phase as

$$f_{\text{vdW}}(T, n_b, Y_q) = f_{\text{ex}}(T, n_b, Y_q) + \Delta f(n_b, Y_q), \quad (12)$$

where Δf models the mean contribution from an attractive potential. It is simpler to specify the free energy difference Δf directly rather than start from the definition of the potential. Because the contribution from the potential separates (see, e.g., Ref. [14]), the two ways of formulating this contribution are practically equivalent. That is, we take [89]

$$\begin{aligned} \Delta f(n_b, Y_q) = &\, f_{\text{cold}}(n_b) \\ &- f_{\text{ex}}(T = 0, n_b, Y_q) \\ &+ f_{\text{HS(DD2)}}(T = 0, n_b, Y_q) \\ &- f_{\text{HS(DD2)}}(T = 0, n_b, Y_q^{\text{eq}}(n_b)), \quad (13) \end{aligned}$$

where f_{cold} is the free energy of the one-dimensional cold hybrid EOS constructed as discussed above, $f_{\text{HS(DD2)}}$ is the free energy of the HS(DD2) model, and Y_q^{eq} is the value at β equilibrium for the HS(DD2) EOS.

The first two lines on the right-hand side of Eq. (13) adjust the dependence of the EOS on n_b such that it matches with the cold hybrid EOS at zero temperature. The last two lines in Eq. (13) adjust the dependence on Y_q such that it agrees with that of the HS(DD2) EOS at low temperatures, without changing the EOS at β equilibrium.

C. Transition between the vdW model and HS(DD2)

At low densities, such as is relevant, for example, in the crust of the neutron stars, the combination of the holographic model with the vdW gas becomes unreliable, so we use instead directly the HS(DD2) EOS. We implement this by switching from the vdW model of Eq. (12), which already borrows the Y_q dependence from HS(DD2), smoothly to the exact HS(DD2) EOS at a well-chosen transition density. However, before this is possible it is necessary to adjust the HS(DD2) EOS by adding the contribution from the mesons of QCD as indicated in Fig. 1. This contribution is important only in the region of low density and high temperatures (i.e., close to the transition temperature in QCD), which is far from the regime relevant for neutron stars and core-collapse supernovae. We however add this contribution since it affects the study of the critical point, which we carry out below. We write the "improved" HS(DD2) EOS as

$$\begin{aligned} \hat{f}_{\text{HS(DD2)}}(T, n_b, Y_q) = &\, f_{\text{HS(DD2)}}(T, n_b, Y_q) \\ &+ \sum_j p_{\text{BE}}^{(j)}(T, m_j), \quad (14) \end{aligned}$$

where the sum goes over all mesons from the particle data group [72] with masses below 1 GeV.

After this modification, we define the final nuclear matter EOS as

$$\begin{aligned} f_{\text{NM}}(T, n_b, Y_q) = &\, [1 - w(n_b)]\hat{f}_{\text{HS(DD2)}}(T, n_b, Y_q) \\ &+ w(n_b)f_{\text{vdW}}(T, n_b, Y_q), \quad (15) \end{aligned}$$

where the weight function is

$$w(n_b) = \frac{1}{2}\left[1 + \tanh\left(\frac{\log(n_b/n_0)}{1.75}\right)\right] = \frac{(n_b/n_0)^{8/7}}{1 + (n_b/n_0)^{8/7}}, \quad (16)$$

with $n_0 \approx 0.0694n_s$. The numerical coefficients were chosen such that the transition from HS(DD2) to vdW is smooth for all temperatures and charge fractions.

D. Mixed phase and the critical point

The final step in our construction is to combine the NM and QM components into a single EOS. In order to do this, we first need to adjust the V-QCD QM result: the EOS constructed in Ref. [54] includes neither dependence on the

charge fraction nor electron pressure. It would be possible to compute the charge fraction dependence from the model directly, but this would require a significant extension of the model, which is beyond the scope of this article in which the focus is on temperature dependence. Therefore we resort to approximations.

There are two simple approximation schemes. The first is to assume that the free energy of strongly interacting matter only depends on the total baryon number, given as the sum over the quark number densities as $n_b = (n_u + n_d + n_s)/3$. In this case the free energy of QM arises as the sum over the electromagnetic contribution and the V-QCD pressure:

$$f_{QM}(T, n_b, Y_q) = f_{e\bar{e}\gamma}(T, Y_q n_b) + f_{\text{V-QCD}}(T, n_b), \quad (17)$$

where the electron density is $n_e = Y_q n_b$ by charge neutrality. The electromagnetic term $f_{e\bar{e}\gamma}$ is estimated as the sum of the ideal gas free energies of electrons, positrons, and photons at the given electron density.

The second scheme (which was used in Ref. [25]) assumes that the free energy arises as a direct sum of the free energies of different quark flavors with equal amount of down and strange quarks. This gives

$$f_{QM}(T, n_b, Y_q) = f_{e\bar{e}\gamma}(T, Y_q n_b) + \frac{1}{3} f_{\text{V-QCD}}(T, (1 + Y_q) n_b)$$
$$+ \frac{2}{3} f_{\text{V-QCD}}(T, (1 - Y_q/2) n_b), \quad (18)$$

where the last term in the first line and the term in the second line are the contributions from up-type and down-type quarks, respectively. Note that this approach includes a simple approximation for the symmetry energy of quark matter, which assumes no interactions between the different quark flavors, and therefore corresponds to the probe limit where the backreaction of the flavors to the gluon dynamics is neglected. However, there is no reason to expect that the effect of the backreaction is small. In this article, we use the simplest approximation of Ref. (17).

The final EOS and phase diagram, including the mixed phase between NM and QM, is then found by carrying out a Gibbs construction, neglecting effects of finite surface tension (see Appendix A 2 for details). As it turns out, two different regimes can be clearly identified from the result. At low temperatures, there is a very strong first-order phase transition, which becomes weaker with increasing temperature. At higher temperatures there is a weak first-order transition. We interpret this weak transition as the signal of crossover: continuity over the phases is not possible because this would require a precise match between the EOS of the meson gas (in the NM phase) with the V-QCD QM EOS. We have not tried to carry out such matching here; this is left for future work. The transition between the two regimes is therefore interpreted as the critical end point of the nuclear to quark matter transition line. We illustrate

the mixed phase and the critical point in detail in Sec. IV and in Appendix C.

IV. RESULTS

We now analyze the thermodynamic properties of the constructed EOS. We have carried out the steps outlined in Sec. III for all three versions of the cold hybrid EOS, leading likewise to three versions of the final equation of state which depends on baryon number density, temperature, and charge fraction. The naming of the models is inherited from the cold EOS, so that we refer to the three EOS as "soft," "intermediate," and "stiff," according to the stiffness (i.e., basically the values of the speed of sound) of the EOS in the region of dense nuclear matter. The stiffness is directly related to the maximal radii and masses of neutron stars described by the corresponding EOS.

Before going to the analysis of our EOS, let us summarize how they agree with known constraints from various sources. Since the V-QCD QM model was fitted to lattice data, good agreement with lattice results at low density, including the first nontrivial Taylor expansion coefficient in the chemical potential, is guaranteed above the crossover temperature, $T \gtrsim 150$ MeV. Because the meson gas contribution is added to HS(DD2) at lower temperatures, agreement with QCD in this opposite region is obtained as well: it is known that even with our simple approximation, good agreement with lattice data, including higher-order Taylor coefficients in chemical potential, is found [75,90–92]. Moreover, the QM EOS agrees by construction [63,64] with leading perturbative QCD results both at high temperatures and high chemical potentials (see Refs. [25,54] for explicit comparison); since V-QCD is a strongly coupled model, more detailed agreement with higher-order perturbative results is not possible. The hybrid EOS, which we use for the cold EOS, agree by construction with models at low density such as chiral effective theory computations. Actually, the cold hybrid EOS are in excellent agreement (see Refs. [19,23]) at all densities with model independent constructions of the EOS such as polytropic interpolations between the known low and high density limits [93–96] (see also Ref. [97]), and consequently also agree with constraints from neutron star measurements and from the GW170817 merger event [98,99]; see, e.g., Ref. [100]. We also discuss these constraints explicitly below. Furthermore, our predictions for cold matter are in remarkably good agreement with the predictions from the functional renormalization group approach [101–103] both in the quark matter and dense nuclear matter phases. Lastly, our model is in good agreement with finite-temperature calculations in chiral effective theory, as we discuss in more detail below.

Let us now discuss some details of the final EOS. Recall that while we mostly illustrate our results at β equilibrium, the constructed EOS are defined for generic charge fractions Y_q and are therefore also valid outside β equilibrium.
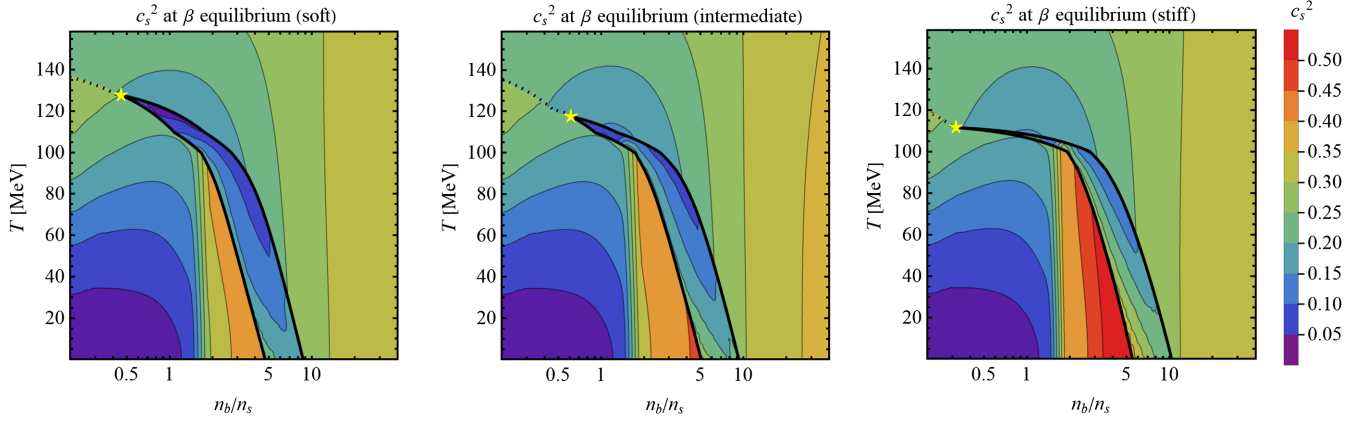
FIG. 2. Contours of the speed of sound squared in β equilibrium for soft (left), intermediate (middle), and stiff (right) EOS. Solid black lines separate the mixed phase from NM and QM phases; yellow stars mark the locations of critical points whose numerical values are listed in Table I.

This is important for applications in neutron star mergers and in heavy-ion collisions. In Fig. 2 we plot the adiabatic speed of sound squared for our three models in β equilibrium as a function of baryon number density and temperature. Solid black lines at intermediate densities represent phase boundaries between baryonic, mixed, and quark phase, while dashed lines correspond to the artificial phase boundary of our construction at low densities and temperatures close to the crossover between baryonic and quark phase in QCD (see Appendix C). The speed of sound squared can be expressed in terms of first derivatives as

$$c_s^2 = \frac{n^2 \left[\left(\frac{s}{n_b} - \frac{\partial s}{\partial n_b} \right)^2 + \frac{\partial s}{\partial T} \frac{\partial \hat{\mu}}{\partial n_b} \right]}{\frac{\partial s}{\partial T} (\epsilon + p)}, \tag{19}$$

where we assumed charge neutrality, and all quantities are assumed to be functions of T, n_b, and Y_q. The chemical potential is defined as $\hat{\mu} = \mu_b + Y_q \mu_l = \partial f / \partial n_b$, where μ_b (μ_l) is the baryon number (electron lepton number) chemical potential. In all three models c_s^2 exceeds the value of $c_{s,\text{CFT}}^2 = 1/3$ in conformal field theory close to the onset of the mixed phase. The maximal values for c_s^2 are 0.42, 0.47, and 0.59 for soft, intermediate, and stiff variants, respectively. The contours in the mixed phase are also determined by Eq. (19), but note that this expression is not the physical speed of sound in this phase.

Yellow stars in Fig. 2 mark the location (T_c, n_{bc}) of the critical point in the respective models whose precise values are listed in Table I. The critical point has been analyzed in various models in the literature, and the results for the location vary in a wide range depending on the model [47,104–106]. Recent results in a simpler holographic approach [47], which extrapolates results for thermodynamics of QCD from lattice QCD to higher values of baryon chemical potential by using a bottom-up setup, are given by $\{T_c, \mu_{bc}\} = \{112, 612\}$ MeV [48]

and $\{T_c, \mu_{bc}\} = \{89, 724\}$ MeV [49,50]. These numbers are in the same ballpark with ours: we obtain on average slightly higher critical temperatures and lower critical chemical potentials. Note also that the critical point in all three variants is outside the regime probed by the second phase of the beam energy scan at RHIC [107], but will be probed in future experiments at FAIR and at NICA. Finally, our numbers lie close to the chemical freeze-out curve extracted from heavy-ion experiments (see, e.g., Refs. [108,109]). Our numbers are actually slightly below the experimental data, but consistent with the curve if the precision of the data and our approach are taken into account.

In Fig. 3 we plot the latent heat $\Delta\epsilon = \epsilon_{\text{QM}} - \epsilon_{\text{NM}}$, i.e., the difference between the energy density in the quark phase ϵ_{QM} and the nuclear matter phase ϵ_{NM}, as a function of the temperature. For the three models we have analyzed, the soft (stiff) model leads to the smallest (largest) latent heat at small temperatures. Curiously, at $T \approx 100$ MeV all three models lead to approximately the same value of $\Delta\epsilon$. The vanishing of the latent heat $\Delta\epsilon = 0$ determines the location of the critical point. As noted above, the phase transition in our model is always of first order, which means $\Delta\epsilon$ does not vanish exactly. However, $\Delta\epsilon$ becomes small above certain temperatures and the point where $\Delta\epsilon = 0$ is obtained via extrapolation (see Appendix C for details).

The temperature T_c of the critical point is correlated with the stiffness of the respective model: larger stiffness results

TABLE I. EOS and neutron star properties in β equilibrium.

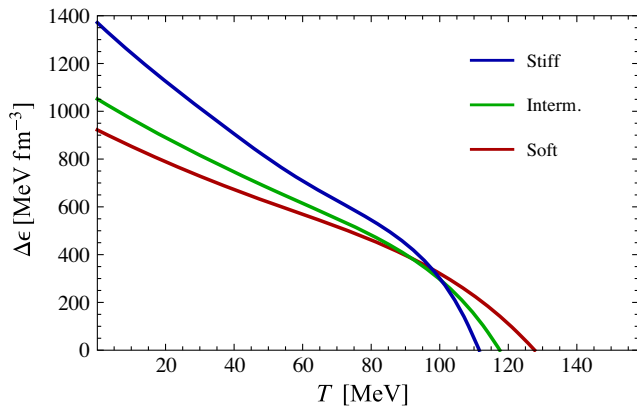| Model	$\frac{n_{bc}}{n_s}$	$\frac{\mu_{bc}}{\text{MeV}}$	$\frac{T_c}{\text{MeV}}$	$\frac{M_{\text{TOV}}}{M_\odot}$	$\frac{R_{e,1.4}}{\text{km}}$	$\Lambda_{1.4}$
Soft	0.46	485	128	2.02	12.41	483
Intermediate	0.62	575	118	2.14	12.50	511
Stiff	0.32	565	112	2.34	12.64	560
HS(DD2)				2.45	13.2	686

FIG. 3. Latent heat as function of T is shown for the three variants of EOS. The location of the critical end point is determined via the condition $\Delta\epsilon(T_c, n_{bc}) = 0$.

in lower values of T_c. However, there is no clear relation between the critical density and stiffness, as the highest value of n_{bc} is found for the intermediate model. In this case we interpret the variation of n_{bc} as a rough measure of the precision for the value of the critical density.

We note that the vdW HG part of our model also captures the critical end point of the liquid-gas transition in the QCD phase diagram. The location of this critical point is around $T = 21$ MeV and $n_b = 0.07$ fm^{-3} for symmetric nuclear matter ($Y_q = 0.5$), which is similar to the predictions of other models in this class [14]. The critical temperature in our construction turns out to be a bit higher than typical numbers, presumably because our potential is determined by the matching to HS(DD2) + APR and therefore different than in other models. However, our value for the critical density agrees well with the numbers in Ref. [14].

In Fig. 4 we plot the pressure as a function of the baryon number density at different values of the temperature in β equilibrium. The lower (upper) bounds of the colored bands represent the soft (stiff) model, while the central curves

correspond to the intermediate version. The results in the nuclear matter phase for $n_b/n_s < 1.4$ are the same for all three models as there is no input from holography in this region. The uppermost curve ($T = 150$ MeV) shows the EOS in the quark matter phase entirely described by V-QCD, which is therefore slightly different for all three models even at low n_b. The plateau at intermediate densities is a manifestation of the strong first-order phase transition of the V-QCD model. The transition density decreases with increasing temperature, and the transition becomes weaker, as also can be seen from Fig. 3.

To illustrate the impact of Y_q outside β equilibrium we plot in Fig. 5 the range in pressure that is covered by the intermediate model at various values of the temperature. Solid curves show the pressure in β equilibrium, while upper and lower bounds of the hatched colored bands are maximum and minimum values, respectively, at given density and temperature. Overall the pressure is lowest close to and increases away from β equilibrium, except close to the onset of the mixed phase, where the pressure can take smaller values also away from β equilibrium. The variation of the pressure as a function of Y_q is largest in the mixed phase.

A quantity that is useful to explore the thermal contributions to the energy density and the pressure is the thermal index defined as

$$\Gamma_{\text{th}}(T, n_b, Y_q) = 1 + \frac{p(T, n_b, Y_q) - p(0, n_b, Y_q)}{\epsilon(T, n_b, Y_q) - \epsilon(0, n_b, Y_q)}. \quad (20)$$

In Fig. 6 we show the thermal index on the β equilibrium slice for various values of the temperature. As in Fig. 4, the upper (lower) bound of the colored bands represents the stiff (soft) model, while the central curves represent the intermediate case. The dashed gray line is the thermal index
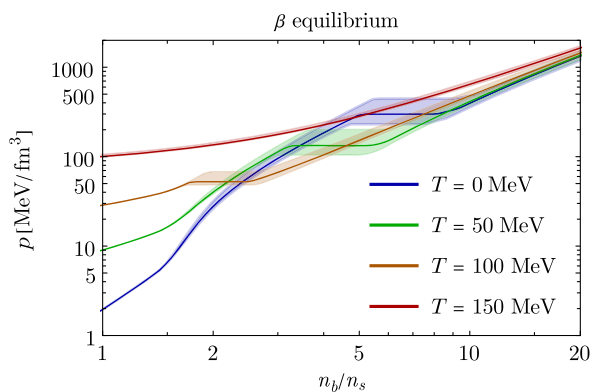

FIG. 4. Pressure as function of the baryon number density in β equilibrium for different values of the temperatures. The lower (upper) bounds of the colored bands represent the soft (stiff) model, while central curves correspond to the intermediate version.
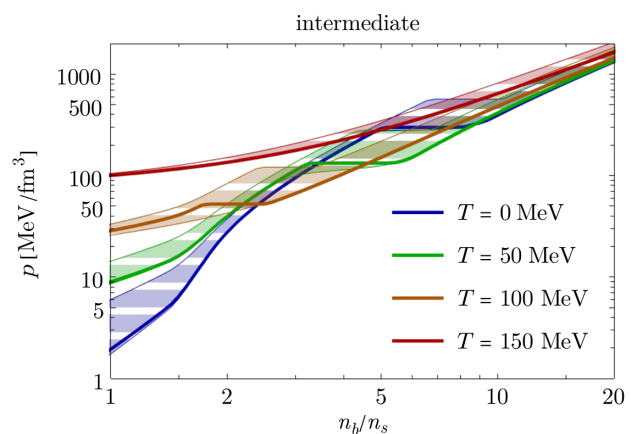

FIG. 5. Pressure for the intermediate model for different values of the temperatures. Solid curves are β equilibrium, while upper and lower bounds of the hatched colored bands represent maximum and minimum values of the pressure at given temperature and density.
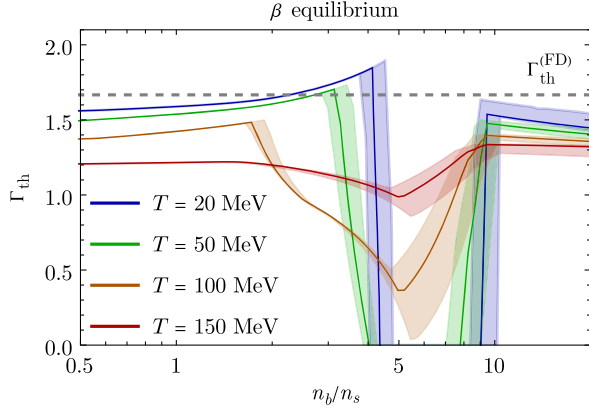
FIG. 6. Thermal index in β equilibrium. Notation for the bands as in Fig. 4.

FIG. 7. Mass-radius relation of nonrotating stars.

of a free Fermi gas $\Gamma_{th}^{(FD)} = 5/3$, which is independent of density and temperature. Any deviations of $\Gamma_{th}(T, n_b, Y_q)$ from $\Gamma_{th}^{(FD)}$ are due to thermal interaction effects. Results for the thermal index were computed at low temperatures and up to densities between $1n_s$ and $2n_s$ by using chiral effective theory in Refs. [1,110]. It is important to compare our EOS to these results in particular because the temperature dependence in our setup in this region is based on the vdW setup, which is not guaranteed to be realistic enough to agree with the CET calculations. Interestingly, our results show good overall agreement with the CET predictions; i.e., deviations are mostly below 10% in the relevant region. Below $\sim 0.5n_s$ the CET predicts values above 1.6 which are slightly higher than our $T = 20$ MeV curve. Also the CET analysis predicts mild decrease of the thermal index with increasing density, whereas in our model the index mildly increases with increasing density. In neutron star simulations a constant thermal index $\Gamma_{th} = 1$–2 is often assumed to mimic such finite-temperature effects [111–113], where $\Gamma_{th} \approx 1.7$ has been argued [114] to best approximate the dynamical and thermodynamical behavior of neutron star merger simulations with microscopic prescription of finite-temperature effects. The thermal index in our construction remains also well within these bounds at temperatures relevant in such simulations, except in and close to the mixed phase, where Γ_{th} can take values smaller than one. As expected, thermal interaction effects become more important at higher temperature, where the deviations of the thermal index from $\Gamma_{th}^{(FD)}$ are largest.

Finally, in Fig. 7 we show the mass-radius relation of cold isolated nonrotating neutron stars for the soft (red), intermediate (green), and stiff (blue) model, together with the relevant observational constraints. Solid parts of the curves represent purely baryonic stars, while dashed parts belong to stars with quark matter cores, which in our model turn out to be unstable. Circles mark the maximum mass of stable nonrotating stars (M_{TOV}) of the respective model.

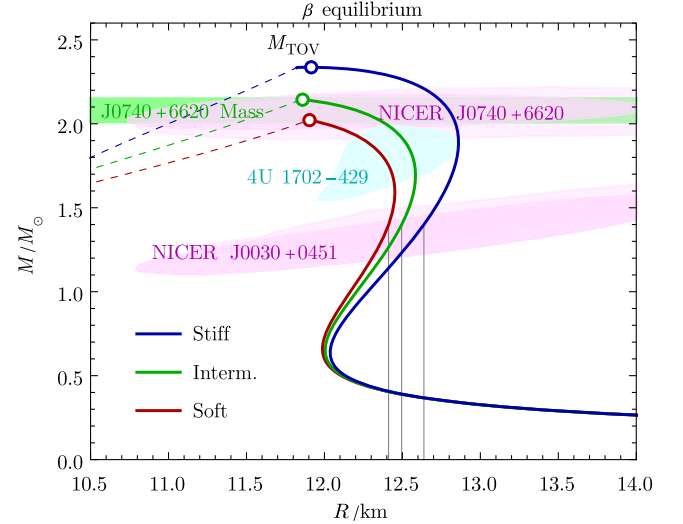For the soft and intermediate model M_{TOV} is determined by the onset of the phase transition at which the star becomes unstable to black hole collapse. For the stiff model the maximum mass is already reached in the baryonic phase, and the phase transition is realized only in the unstable branch of the mass-radius sequence. The green band shows the result $M_{TOV} = 2.08 \pm 0.07 \, M_{\odot}$ from direct mass measurements of the pulsar J0740 + 6620 [115,116], which sets a lower bound on the maximum mass of nonrotating neutron stars. Pink ellipses are radius measurements from the NICER experiment for the pulsars J0030 + 0451 [117,118] and J0740 + 6620 [119,120], while the cyan area is from the measurement of the x-ray binary 4U 1702-429 [121]. All three examples pass the observational constraints shown in the plot in addition to the constraint on the tidal deformability $\Lambda_{1.4} < 580$ of a $M = 1.4 \, M_{\odot}$ star deduced from the analysis of GW170817 by LIGO-Virgo (low-spin prior at 90% confidence level) [122] (see also Table I and the detailed analysis in Ref. [23]).

V. CONCLUSION AND OUTLOOK

In this article, we presented a novel framework for the EOS of hot and dense QCD which combines ingredients from various approaches in different regions of the phase diagram including gauge/gravity duality, van der Waals model of nuclear matter, statistical models, and relativistic mean-field theory. The aim was to establish an EOS which uses the best available modeling in each of the regimes. An essential new input here was the holographic V-QCD model, which we used to cover the region of intermediate densities where computing theoretical predictions is particularly hard. We presented three versions of the EOS which are in good agreement with QCD data and constraints from measurements of neutron stars and neutron

star mergers. Using these models we derived, apart from the properties of the EOS itself, predictions for the location of the critical end point of the nuclear to quark matter transition.

Some details in our approach merit further study. It is expected (see, e.g., Ref. [123]) that at low temperatures in the quark matter phase, pairing of quarks takes place, leading to a potentially complex phase diagram with various paired, color superconducting phases. Recently, there has been a lot of interest in the analysis of such phases in gauge/gravity duality [124–129]. Future work will study the inclusion of such phases in the V-QCD model and their effect on the EOS.

While the main focus in this article was the temperature dependence, we also included the dependence on the charge fraction following the HS(DD2) model in the nuclear matter phase, and by using a simple approximation assuming a strongly interacting component of free energy only depending on the total baryon number (and with free electron gas) in the quark matter phase. This latter approach can be improved by including proper flavor dependence in the holographic model, so that one can consider states with unequal amount of different quark flavors. This extension of the model is the topic of ongoing research.

The inclusion of flavor dependence will also help to generalize the model to analyze transport properties of QCD matter, at least in the region covered by V-QCD. The strongly interacting components of conductivities and viscosities of QM at high density were solved in Refs. [130,131]. Including flavor dependence will help to properly analyze the correlators of electric and weak currents, which are necessary to estimate the effects of electron and neutrino transport, known to be important, among other things, for neutron star cooling, in core-collapse supernovae, and for the behavior of ejected matter in neutron star mergers (see, e.g., Ref. [132]).

We also want to comment on the impact of surface tension in the mixed phase, which we have neglected in this work. In general, first-order phase transitions proceed as a dynamic bubble nucleation process, which cannot be necessarily described in terms of a single equation of state. However, the corresponding surface tension can in principle be computed in the V-QCD model, but the calculation is technically extremely difficult. Such calculations have been carried out for the deconfinement transition in a different gauge/gravity model (without quarks) in Ref. [133]. In this case the value of the surface tension (or more precisely, the corresponding contribution to the energy density at the domain wall) is clearly suppressed with respect to the latent heat. Our values for the latent heat in Fig. 3 are also clearly larger than the estimates of Refs. [53,134] assuming any reasonable estimates for the domain wall width. In summary, we expect surface tension to play a minor role in our setup, but it would certainly be desirable to substrate our expectation by an explicit calculation. Similarly, it

would be interesting to study how important Coulomb effects [135] are in our setup.

We should stress that the framework presented here admits immediate natural generalizations where one replaces some of the building blocks of the model by other approaches. As for the strongly coupled gauge/gravity duality model, there is (to our knowledge) currently no alternative to V-QCD that would allow one to repeat the analysis as done in this article. This field is however evolving rapidly [136–142]. For example, very recently it was demonstrated that a setup with nuclear matter in the Witten-Sakai-Sugimoto model may lead to realistic neutron stars [143]. For the temperature dependence of dense nuclear matter, we used the vdW model for two reasons: it is simple and agrees reasonably well with the holographic model at zero temperature. A simple model may be the best guess for the temperature dependence at densities around and above the saturation density, where none of the known approaches are reliable. However, other choices are also possible. We have checked that using (for example) the temperature dependence of the HS(DD2) model instead only leads to rather mildly modified EOS. It would also be interesting to study the Carnahan-Starling generalization of the excluded volume effect in the vdW model, recently considered in Ref. [28], since it may improve the temperature dependence of the EOS at low but nonzero temperatures near the saturation density, where *ab initio* results are available. Another simple generalization of our approach is to use some other general purpose EOS for the low density region than the HS(DD2) model.

The focus in the construction of our EOS model was on the parameter space of low or intermediate temperature and high density that is relevant for neutron star simulations, but in principle the model can also be applied in the context of heavy-ion collisions. However, in its current version there are some limitations to this, due to the rather simple description of the hadronic phase near the crossover region at low densities in terms of the (HS)DD2 EOS in combination with a free meson gas. This part of the model could be improved, e.g., by gluing in the methods of Ref. [14] in the relevant region of the phase diagram, or by extending the methods of Ref. [67] to finite density. Recall that the current model has a weak first-order phase transition at low densities instead of a crossover, which could be improved in such extensions of the model. We plan to prepare and provide EOS tables dedicated to heavy-ion collisions with improved resolution in the low density and high temperature region around the critical point in the future.

Apart from varying the building blocks of the model, a future study could further explore the parameter space of the model presented in this article. Recall that here we restricted to the main uncertainty of our construction, which arises from the precise choice of the holographic V-QCD action. Therefore, the extended study would mean including additional variants of the V-QCD model [54],

studying the effect of varying the excluded volume parameter v_0 in the vdW model, analyzing the dependence on the choices of matching densities between the building blocks, and finally the dependence on the parameters of the low density nuclear theory model, which could perhaps most easily be done by replacing HS(DD2) by a set of models from the literature.

The EOS constructed in this article will be published in the standard format in the CompOSE database, and can therefore immediately be used in state-of-the-art simulations of neutron star mergers and core-collapse supernovae. Indeed, there is growing interest in effects arising due to the temperature dependence and the phase transition in merger simulations [2,7,43,144]. Work on applying the EOS of this article in such simulations is already in progress.

APPENDIX A: TECHNICAL DETAILS ON THE EOS

In this appendix, we discuss minor technical details which are not important for our conclusions but need to be discussed for all the results to be fully reproducible.

1. Details of the construction of the cold EOS

We first give more details on the construction of the cold hybrid EOS. Recall that the EOS of cold nuclear matter, as explained in Sec. III A, requires matching between EOS from a nuclear theory model (in this article, the APR model) at low density with V-QCD nuclear matter at higher density. As we explained in the main text, in order for the cold EOS to be smoother, we choose two matching densities, instead of the single density approach of Refs. [18,19], and connect the speeds of sound from the two approaches through a linear interpolation of the squared speed of sound c_s^2 as a function of the baryon

number density n_b, therefore avoiding a discontinuity in the speed of sound.

To be precise, the matching is carried out as follows. For $n_b < 1.4n_s \equiv n_{\rm tr}^{(1)}$ we use the APR EOS as such. We then take the speed of sound for $n_{\rm tr}^{(1)} < n_b < 1.8n_s \equiv n_{\rm tr}^{(2)}$ to be

$$[c_s(n_b)]^2 = \left[c_s\left(n_{\rm tr}^{(1)}\right)\right]^2 + \kappa(n - n_{\rm tr}^{(1)}), \qquad (A1)$$

where the slope κ is a free parameter. The rest of the thermodynamic functions are then obtained by integration for $n_{\rm tr}^{(1)} < n_b < n_{\rm tr}^{(2)}$ so that κ is the only free parameter. We then require that the pressure, the baryon number chemical potential, and the speed of sound are continuous at $n_b = n_{\rm tr}^{(2)}$. These three conditions then determine κ as well as the two parameters of V-QCD nuclear matter c_b and b [these parameters appear in the nuclear matter action $S_{\rm NM}$ of Eq. (1); see Ref. [19] for their definitions]. These latter two parameters were also determined by matching in the simpler approach of Refs. [18,19].

We also modify the cold hybrid EOS in the crust region, $n_b \ll n_s$, before using it to construct the adjusted vdW EOS through Eq. (13), in order to remove some noise from the vdW EOS. This noise would appear because the fine details of the β-equilibrium, zero temperature APR EOS, which turns out to be inconsistent with the Y_q dependence of the HS(DD2) EOS at low density. One might wonder why we need to do this, since we replace the vdW EOS with the exact HS(DD2) through Eq. (15) at low densities. However, since we use a smooth weight function instead of an abrupt cutoff, noise in the vdW EOS at low densities would remain in the final matched EOS even if it would be heavily suppressed. We therefore implement the correction by using the HS(DD2) at β equilibrium for the cold EOS $f_{\rm cold}(n_b)$ when $n_b < 0.008n_s$. At this value the pressures of the APR and HS(DD2) EOS cross, and we further introduce a small shift in the baryon chemical potential for $n_b < 0.008n_s$ in order to make it continuous at $n_b = 0.008n_s$. That is, we in effect introduce a second-order phase transition. We stress, however, that these modifications only remove noise from heavily suppressed terms at low density in our final results.

2. Details of the construction of the three-dimensional EOS

We now discuss some technical details on the determination of the final three-dimensional EOS and its components.

We carried out some minor but nontrivial modifications in the three-dimensional nuclear matter EOS $f_{\rm NM}(T, n_b, Y_q)$. The transition from nonuniform to uniform nuclear matter in HS(DD2) proceeds via a first-order phase transition at around $0.3n_s \lesssim n_b \lesssim 0.5n_s$, at small temperatures $T \leq 5$ MeV, and values of Y_q (mostly) far from β

equilibrium [15]. Because of the smooth matching of Eq. (15), the mixed phase from this transition causes the resulting nuclear matter to be inconsistent in this narrow range of parameters, so that a thermodynamically unstable region appears. In order to fix this, we carried out a simple one-dimensional Maxwell construction for each value of T and Y_q which removed the inconsistency.

Let us also specify how the EOS for the mixed phase between the NM and QM phases was calculated. It arises from requiring full chemical equilibrium, so that the coexisting phases have the same pressure as well as baryon number and electron lepton number chemical potentials:

$$\mu_l = \frac{1}{n_b} \frac{\partial f}{\partial Y_q}\bigg|_{n_b, T}, \qquad (A2)$$

$$\mu_b = \frac{\partial f}{\partial n_b}\bigg|_{n_b Y_q, T} = \frac{\partial f}{\partial n_b}\bigg|_{Y_q, T} - Y_q \mu_l. \qquad (A3)$$

In practice, the mixed phase is found as follows. Demanding equilibrium between the phases, we need to solve the following set of equations:

$$p_{\mathrm{NM}}(T, n_b^{(1)}, Y_q^{(1)}) = p_{\mathrm{QM}}(T, n_b^{(2)}, Y_q^{(2)}), \qquad (A4)$$

$$\mu_b^{(\mathrm{NM})}(T, n_b^{(1)}, Y_q^{(1)}) = \mu_b^{(\mathrm{QM})}(T, n_b^{(2)}, Y_q^{(2)}), \qquad (A5)$$

$$\mu_l^{(\mathrm{NM})}(T, n_b^{(1)}, Y_q^{(1)}) = \mu_l^{(\mathrm{QM})}(T, n_b^{(2)}, Y_q^{(2)}). \qquad (A6)$$

We have three conditions and four variables $n_b^{(i)}$, $Y_q^{(i)}$, so the solution will involve one parameter which we call γ. The solution defines two curves on the (n_b, Y_q) plane, parametrized in terms of γ, and a mapping between the curves. The mixed phase is found between the curves. The temperature is a "trivial" parameter in these equations and we will not denote the dependence on it explicitly below. The construction can be carried out independently for each value of the temperature.

The mixed phase is then a mixture of NM and QM matter in the equilibrium defined by Eqs. (A4)–(A6). The thermodynamic functions are most easily written in a parametric representation using the γ parameter and the volume fraction α of the NM phase. That is, we may write

$$n_b(\alpha, \gamma) = \alpha n_b^{(1)}(\gamma) + (1 - \alpha) n_b^{(2)}(\gamma), \qquad (A7)$$

$$\begin{aligned} Y_q(\alpha, \gamma) n_b(\alpha, \gamma) &= \alpha Y_q^{(1)}(\gamma) n_b^{(1)}(\gamma) \\ &\quad + (1 - \alpha) Y_q^{(2)}(\gamma) n_b^{(2)}(\gamma), \end{aligned} \qquad (A8)$$

$$\begin{aligned} f(\alpha, \gamma) &= \alpha f_{\mathrm{NM}}(n_b^{(1)}(\gamma), Y_q^{(1)}(\gamma)) \\ &\quad + (1 - \alpha) f_{\mathrm{QM}}(n_b^{(2)}(\gamma), Y_q^{(2)}(\gamma)) \end{aligned} \qquad (A9)$$

separately for each temperature slice. Note that curves of constant γ are straight lines on the $(n_b, Y_q n_b)$ plane. By construction, p, μ_b, and μ_l take constant values on these lines.

Note that in the main text we focused on defining the free energy, which is the natural thermodynamic potential in the canonical ensemble with the parameters T, n_b, and Y_q. Determining first numerically the free energy, and computing the other thermodynamic functions by using it as input, is indeed enough to determine all thermodynamics. However, this procedure requires taking numerical derivatives, which tend to increase numerical noise. When computing the final results for other observables (such as the entropy and the chemical potentials), we have therefore first computed analytically the consequences of the various matching formulas, and computed these quantities directly from the corresponding quantities of the EOS being matched, avoiding the use of numerical derivatives as much as possible.

APPENDIX B: COMPARISON OF THE vdW EOS TO THE V-QCD NM EOS

A central motivation for the use of the vdW EOS in this article is its agreement with the predicted EOS of cold NM by V-QCD. In this appendix, we study this by comparing the three different versions of the cold hybrid V-QCD (APR) EOS to simple vdW EOS, i.e., those only with electrons, protons, and neutrons with a constant excluded volume correction for the nucleons.

The EOS are compared in Fig. 8. In both panels, stiff, intermediate, and soft variants of V-QCD EOS up to the onset of the phase transition are shown via blue, green, red curves, respectively, and simple vdW EOS with EV parameter $v_0 = 0.56$ fm^{-3} (our choice), $v_0 = 1$ fm^{-3}, and $v_0 = 1.5$ fm^{-3} are denoted by solid black, dotted, and dashed curves. The figure on the left shows the baryon chemical potential dependence of the dimensionless pressure p/μ_b^4, and the figure on the right shows the pressure as a function of the baryon number density. The gray curve in the right-hand side plot shows the ideal hadron gas result. This curve is not shown in the left-hand plot since it mostly stays outside the plotted range. It is transparent from the figure that the chemical potential dependence is more sensitive to v_0 at small values of the parameter.

We note that the EV corrected EOS is relatively close to the cold hybrid V-QCD EOS, in particular when the pressure is plotted as a function of the chemical potential. This happens in part because the left-hand plot of Fig. 8 focuses in the region of higher densities where agreement is better. Note that the range of values of v_0 is typical for EV corrections in nuclear matter; see, e.g., Ref. [76]. The best fit between the EV corrected pressure and V-QCD is found around $v_0 \approx 1.5$ fm^{-3}. We however choose a smaller value $v_0 \approx 0.56$ fm^{-3}, because for this value, the potential term of
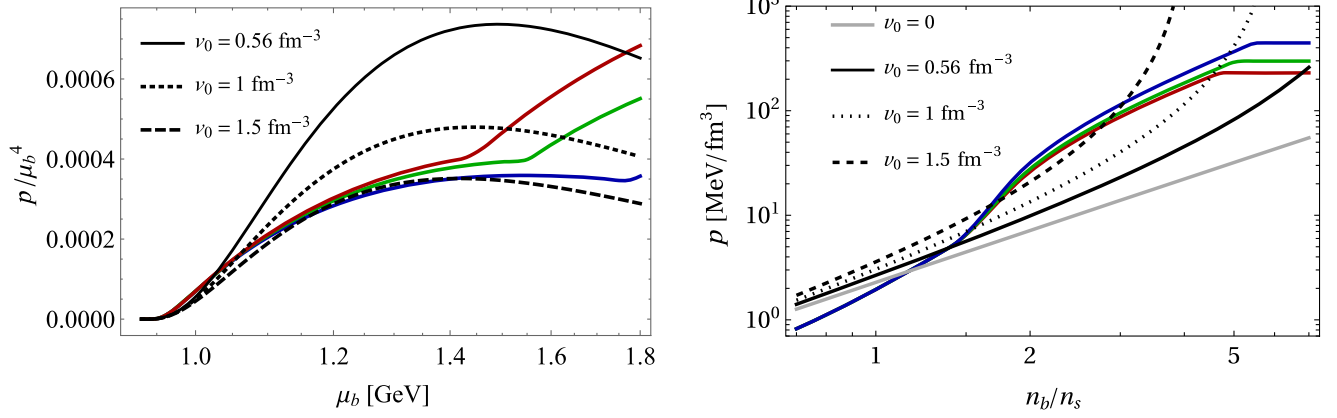
FIG. 8. Comparison of cold V-QCD EOS and EOS of hadron gas with excluded volume correction. Left: normalized pressure (p/μ_b^4) in terms of baryon chemical potential μ_b. Right: pressure in terms of baryon number density n_b in units of n_s. In both panels, stiff, intermediate, and soft variants are denoted by blue, green, and red curves, respectively, and hadron gas with excluded volume of $v_0 = 0.56$ fm^{-3}, $v_0 = 1$ fm^{-3}, and $v_0 = 1.5$ fm^{-3} are exhibited by solid, dotted, and dashed black curves. In addition, ideal hadron gas result is shown with the gray solid curve in the panel on the right.

Eq. (13) is more natural: this value corresponds to a potential which is attractive (repulsive) at long (short) distances, whereas for larger v_0 the potential would be attractive at both short and long distances with an intermediate repulsive range in between. This unnatural behavior is reflected in the nonmonotonic dependence of the pressure difference between the EV corrected and V-QCD pressures as a function of n_b in the left-hand plot of Fig. 8.

APPENDIX C: DETERMINATION OF THE CRITICAL POINT

As discussed in Sec. III D, the EOS have a strong phase transition at low temperature that becomes weaker at higher temperature. Continuity over the phases is not possible due to limitation of our construction. Hence, we interpret the weakening in the transition as a signal for a crossover at high temperature. Using this interpretation, it is possible to calculate the latent heat and obtain an estimate for the location of the critical end point. The latent heat is

$$\Delta\epsilon(T) = \epsilon_{\mathrm{QM}}(T, n_b^{(2)}, Y_q^{\mathrm{eq}}(n_b^{(2)})) - \epsilon_{\mathrm{NM}}(T, n_b^{(1)}, Y_q^{\mathrm{eq}}(n_b^{(1)})),$$
(C1)

where Y_q^{eq} is the value at β equilibrium and $n_b^{(2)}$, $n_b^{(1)}$ are, respectively, the values for the baryon number density at the onset and the end of the phase transition for a given value of T. Because of the absence of a crossover, the transition lines get close, but do not intersect. However, the latent heat as a function of temperature shows a clean trend. By using it, we perform a fifth-order polynomial fit to the data in the range of strong first-order transition, i.e., $T \lesssim 115$ MeV. The fit functions that we obtained are

$$\Delta\epsilon_{\mathrm{stiff}} = 1.37 \times 10^3 - 1.41 \times 10T + 1.53 \times 10^{-1}T^2$$
$$- 4.36 \times 10^{-3}T^3 + 6.26 \times 10^{-5}T^4$$
$$- 3.10 \times 10^{-7}T^5,$$
$$\Delta\epsilon_{\mathrm{interm}} = 1.05 \times 10^3 - 8.85T + 5.01 \times 10^{-2}T^2$$
$$- 9.04 \times 10^{-4}T^3 + 1.28 \times 10^{-5}T^4$$
$$- 7.53 \times 10^{-8}T^5,$$
$$\Delta\epsilon_{\mathrm{soft}} = 9.23 \times 10^2 - 7.07T + 1.40 \times 10^{-2}T^2$$
$$- 2.90 \times 10^{-4}T^3 - 3.40 \times 10^{-6}T^4$$
$$+ 1.53 \times 10^{-9}T^5.$$

The critical temperature is then found by extrapolating to the point where the latent heat vanishes: $\Delta\epsilon(T_c) = 0$. To determine the value of the baryon number density at the critical end point n_{bc}, we use the geometric mean of the density values on the two transition lines at T_c. We estimate the uncertainty of this procedure to be below $0.05n_s$ for the soft EOS and $0.1n_s$ for the intermediate and stiff EOS by studying the variation caused by varying the choice of the mean. While this uncertainty is arguably sizable, it is smaller than the differences between the numbers for the different EOS in Table I. Then for the phase diagram, crossover (dashed) lines are also computed by calculating the geometric mean of n_b on the transition lines at the temperature values above T_c.

APPENDIX D: COMPARISON TO OTHER EOS MODELS

In this appendix, we compare the three V-QCD EOS variants introduced in the main text with a selection of other temperature-dependent EOS. For the comparison, we chose several different nuclear theory models which are widely
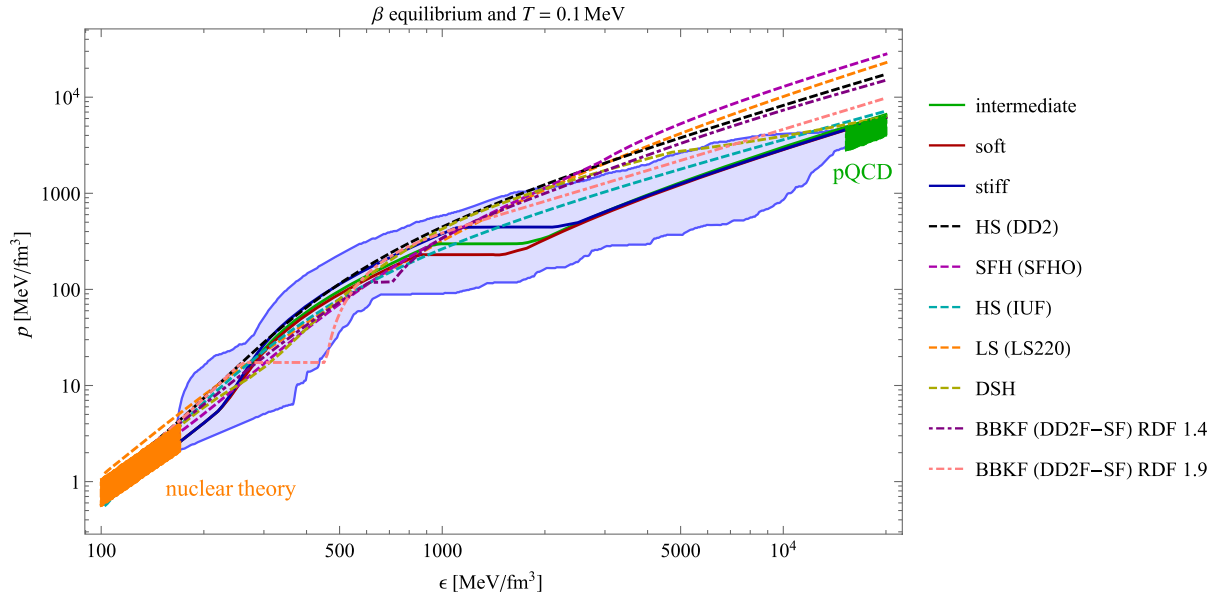
FIG. 9. Comparison of the three variants of V-QCD finite EOS and the chosen set of the other existing finite-temperature nuclear theory EOS: energy density dependence of β-equilibrium pressure at low temperature. Orange and blue bands show the uncertainties in pressure in nuclear theory [154] and perturbative QCD (pQCD) [155], respectively. Blue band indicates all EOS satisfying astrophysical constraints [156].

used in astrophysical applications: HS(DD2) [15,16,145], Steiner-Fischer-Hempel (SFH) (SFHO) [15,83,145], HS (IUF) [15,146,147], Lattimer-Swesty (LS) (LS220) [148,149], Du-Steiner-Holt (DSH) [150,151], and Bastian-Blaschke-Kaltenborn-Fischer relativistic density functional BBKF(DD2F-SF) RDF 1.4 and BBKF(DD2F-SF) RDF 1.9 [15,152]. The tabulated data for these EOS are publicly available in the online databases [22,153]. The comparison is presented in Figs. 9 and 10. In all the plots, stiff, intermediate, and soft V-QCD variants are shown as solid blue, red, and green curves, respectively, while the other EOS without (with) phase transitions are shown as dashed (dot-dashed) curves.

In Fig. 9, we show β-equilibrium pressure as a function of energy density at low temperature. In the figure, uncertainties in nuclear theory [154] and perturbative QCD [155] are marked by orange and green bands. The light blue band encloses all EOS that are consistent with the astrophysical constraints [156]. While most of the EOS are consistent with the bands in low and intermediate density, V-QCD variants are the only ones that meet with uncertainty band of perturbative QCD.

In the top row of Fig. 10, we plot the pressure in β equilibrium as a function of the baryon number density at low (left) and intermediate temperature (right). In the low density regime ($n_b \lesssim n_s$) the pressure of the V-QCD models is lower than in the other EOS. This is because we use the relatively soft APR model in this regime of our hybrid construction, which is necessary to satisfy the constraint on the tidal deformability obtained from the binary neutron star merger event GW170817 (see discussion in the main text).

Another important difference is that the stiffness of the V-QCD baryon part, indicated by the slope of the pressure, rises significantly faster in the intermediate density regime ($n_s < n_b < n_b^{(1)}$) than in the other models. However, the stiffness and the pressure of stiff V-QCD and HS(DD2) are similar in this regime, in particular at intermediate temperature (right-hand plot), where the blue and dashed black line become almost identical. The most prominent difference is the plateau in pressure at high density ($n_b^{(1)} < n_b < n_b^{(2)}$) due to the strong first-order phase transition in the V-QCD model. BBKF(DD2F-SF) RDF 1.4 and BBKF(DD2F-SF) RDF 1.9 (dot-dashed curves) also have similar plateaus since they are hadron-quark models with the first-order phase transition. However, the phase structure of these models is very different than V-QCD predictions. The phase transition in these models occurs at much lower temperature and baryon number density values. There is even no hadronic phase in low density intermediate temperature in BBKF (DD2F-SF) RDF 1.9. The properties of the pure quark matter phases ($n_b > n_b^{(2)}$) in the three V-QCD variants are very similar. However, the pressure and stiffness of V-QCD quark matter are significantly lower than those of the other models including the quark-hadron models. The soft V-QCD quark matter phase and the predicted large latent heat when crossing the mixed phase have important consequences on the collapse time of binary neutron star merger remnants and the emitted gravitational wave signal, as we have demonstrated recently in Ref. [157].

In the left-hand panel of the bottom row, we plot the β-equilibrium pressure as a function of temperature
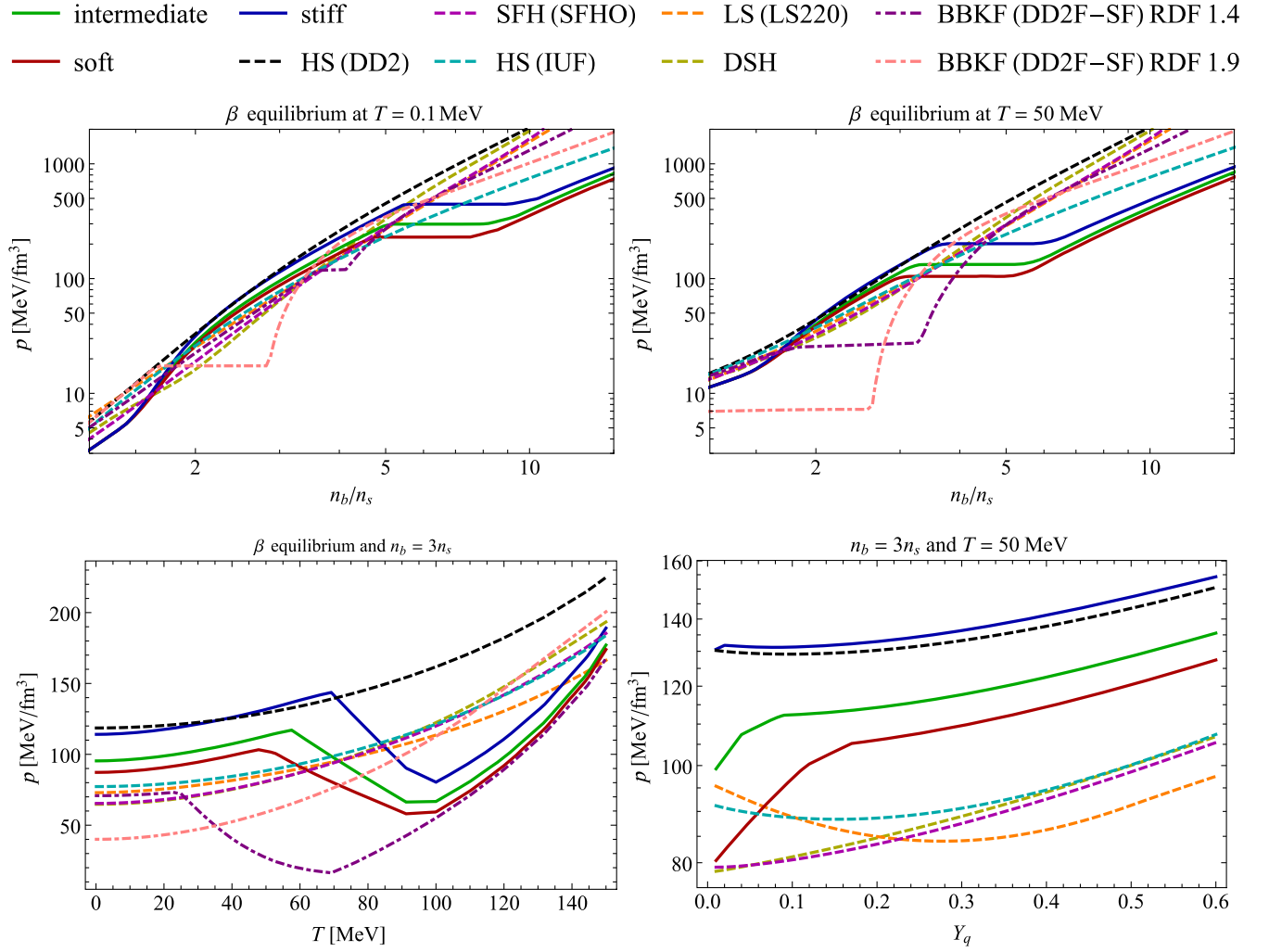
FIG. 10. Comparison of the three variants of V-QCD finite EOS and the chosen set of the other existing finite-temperature nuclear theory EOS: baryon number density dependence of β-equilibrium pressure at low temperature (top left) and intermediate temperature (top right), temperature dependence of β-equilibrium pressure at $n_b = 3n_s$ (bottom left), charge fraction dependence of pressure at $n_b = 3n_s$ and $T = 50$ MeV (bottom right).

at $n_b = 3n_s$. Until the onset of the phase transition, the pressure in the three versions of V-QCD is larger than in the other nuclear theory models, with the exception of HS (DD2). After the onset of the phase transition, this trend changes: the V-QCD pressure decreases until it reaches the end of the mixed phase at $T \approx 100$ MeV, while the pressure in the nuclear matter models keeps increasing monotonically with temperature. Finally, in the pure quark matter phase the pressure starts rising again monotonically with T and reaches comparable values as the other models around $T \approx 150$ MeV (we also note that the BBKF hadron-quark models exhibit qualitatively similar behavior with V-QCD variants in this regime). In the right-hand panel we plot the pressure at $n_b = 3n_s$ and $T = 50$ MeV as a function of the charge fraction. The curves for the hadron-quark models are excluded in the plot since their

pressures are much lower than the other models [maximum values are $p \approx 45$ MeV/fm³ and $p \approx 65$ MeV/fm³ for BBKF(DD2F-SF) RDF 1.4 and BBKF(DD2F-SF) RDF 1.9, respectively]. Different nuclear models exhibit different trends. V-QCD variants and HS(DD2) have significantly larger pressure than the other nuclear matter models. Since the Y_q dependence of our V-QCD hybrids is inherited from HS(DD2), these models have qualitatively similar behavior in the relevant region—the dip of the V-QCD curves at small Y_q is due to the mixed phase. However, intermediate and soft V-QCD have lower pressure than HS(DD2) in the whole Y_q range. Finally, comparing the top and bottom row of Fig. 10 shows that the density dependence of the pressure dominates, while the dependence on temperature and the charge fraction are much weaker.

[1] J. Keller, C. Wellenhofer, K. Hebeler, and A. Schwenk, *Neutron Matter at Finite Temperature Based on Chiral Effective Field Theory Interactions*, Phys. Rev. C **103**, 055806 (2021).

[2] E. R. Most, L. J. Papenfort, V. Dexheimer, M. Hanauske, S. Schramm, H. Stöcker, and L. Rezzolla, *Signatures of Quark-Hadron Phase Transitions in General-Relativistic Neutron-Star Mergers*, Phys. Rev. Lett. **122**, 061101 (2019).

[3] A. Perego, S. Bernuzzi, and D. Radice, *Thermodynamics Conditions of Matter in Neutron Star Mergers*, Eur. Phys. J. A **55**, 124 (2019).

[4] A. Endrizzi, A. Perego, F. M. Fabbri, L. Branca, D. Radice, S. Bernuzzi, B. Giacomazzo, F. Pederiva, and A. Lovato, *Thermodynamics Conditions of Matter in the Neutrino Decoupling Region during Neutron Star Mergers*, Eur. Phys. J. A **56**, 15 (2020).

[5] P. Hammond, I. Hawke, and N. Andersson, *Thermal Aspects of Neutron Star Mergers*, Phys. Rev. D **104**, 103006 (2021).

[6] A. Figura, F. Li, J.-J. Lu, G. F. Burgio, Z.-H. Li, and H. J. Schulze, *Binary Neutron Star Merger Simulations with Hot Microscopic Equations of State*, Phys. Rev. D **103**, 083012 (2021).

[7] C. A. Raithel, V. Paschalidis, and F. Özel, *Realistic Finite-Temperature Effects in Neutron Star Merger Simulations*, Phys. Rev. D **104**, 063016 (2021).

[8] J. Adam *et al.* (STAR Collaboration), *Nonmonotonic Energy Dependence of Net-Proton Number Fluctuations*, Phys. Rev. Lett. **126**, 092301 (2021).

[9] T. Ablyazimov *et al.* (CBM Collaboration), *Challenges in QCD Matter Physics—The Scientific Programme of the Compressed Baryonic Matter Experiment at FAIR*, Eur. Phys. J. A **53**, 60 (2017).

[10] M. Durante *et al.*, *All the Fun of the FAIR: Fundamental Physics at the Facility for Antiproton and Ion Research*, Phys. Scr. **94**, 033001 (2019).

[11] A. N. Sissakian and A. S. Sorin (for the NICA Collaboration), *The Nuclotron-Based Ion Collider Facility (NICA) at JINR: New Prospects for Heavy Ion Collisions and Spin Physics*, J. Phys. G **36**, 064069 (2009).

[12] M. Järvinen and E. Kiritsis, *Holographic Models for QCD in the Veneziano Limit*, J. High Energy Phys. 03 (2012) 002.

[13] T. Ishii, M. Järvinen, and G. Nijs, *Cool Baryon and Quark Matter in Holographic QCD*, J. High Energy Phys. 07 (2019) 003.

[14] V. Vovchenko, *Hadron Resonance Gas with van der Waals Interactions*, Int. J. Mod. Phys. E **29**, 2040002 (2020).

[15] M. Hempel and J. Schaffner-Bielich, *Statistical Model for a Complete Supernova Equation of State*, Nucl. Phys. **A837**, 210 (2010).

[16] S. Typel, G. Ropke, T. Klahn, D. Blaschke, and H. H. Wolter, *Composition and Thermodynamics of Nuclear Matter with Light Clusters*, Phys. Rev. C **81**, 015803 (2010).

[17] A. Akmal, V. R. Pandharipande, and D. G. Ravenhall, *The Equation of State of Nucleon Matter and Neutron Star Structure*, Phys. Rev. C **58**, 1804 (1998).

[18] C. Ecker, M. Järvinen, G. Nijs, and W. van der Schee, *Gravitational Waves from Holographic Neutron Star Mergers*, Phys. Rev. D **101**, 103006 (2020).

[19] N. Jokela, M. Järvinen, G. Nijs, and J. Remes, *Unified Weak and Strong Coupling Framework for Nuclear Matter and Neutron Stars*, Phys. Rev. D **103**, 086004 (2021).

[20] Our construction also captures the first-order liquid-gas transition which we do not show in the illustration, because it is located at such low temperatures making it difficult to display on the same scale as the deconfinement transition, which is the main focus of this work.

[21] S. Typel, M. Oertel, and T. Klähn, *CompOSE CompStar Online Supernova Equations of State Harmonising the Concert of Nuclear Physics and Astrophysics compose .obspm.fr*, Phys. Part. Nucl. **46**, 633 (2015).

[22] https://compose.obspm.fr/.

[23] N. Jokela, M. Järvinen, and J. Remes, *Holographic QCD in the NICER Era*, Phys. Rev. D **105**, 086005 (2022).

[24] T. Demircik, C. Ecker, and M. Järvinen, *Rapidly Spinning Compact Stars with Deconfinement Phase Transition*, Astrophys. J. Lett. **907**, L37 (2021).

[25] P. M. Chesler, N. Jokela, A. Loeb, and A. Vuorinen, *Finite-Temperature Equations of State for Neutron Star Mergers*, Phys. Rev. D **100**, 066027 (2019).

[26] N.-U. F. Bastian and D. B. Blaschke, *A Unified Quark-Nuclear Matter Equation of State from the Cluster Virial Expansion within the Generalized Beth–Uhlenbeck Approach*, Eur. Phys. J. A **57**, 35 (2021).

[27] T. Beisitzer, R. Stiele, and J. Schaffner-Bielich, *Supernova Equation of State with an Extended SU(3) Quark-Meson Model*, Phys. Rev. D **90**, 085001 (2014).

[28] Y. Fujimoto, K. Fukushima, Y. Hidaka, A. Hiraguchi, and K. Iida, *Equation of State of Neutron Star Matter and Its Warm Extension with an Interacting Hadron Resonance Gas*, arXiv:2109.06799.

[29] N. Yasutake and K. Kashiwa, *Lepton Effects on the Proto-Neutron Stars with the Hadron-Quark Mixed Phase in the Nambu-Jona-Lasinio Model*, Phys. Rev. D **79**, 043012 (2009).

[30] K. Masuda, T. Hatsuda, and T. Takatsuka, *Hadron–Quark Crossover and Hot Neutron Stars at Birth*, Prog. Theor. Exp. Phys. **2016**, 021D01 (2016).

[31] T. Kojo, D. Hou, J. Okafor, and H. Togashi, *Phenomenological QCD Equations of State for Neutron Star Dynamics: Nuclear-2SC Continuity and Evolving Effective Couplings*, Phys. Rev. D **104**, 063036 (2021).

[32] I. Bombaci, G. Lugones, and I. Vidana, *Effects of Color Superconductivity on the Nucleation of Quark Matter in Neutron Stars*, Astron. Astrophys. **462**, 1017 (2007).

[33] O. E. Nicotra, M. Baldo, G. F. Burgio, and H. J. Schulze, *Hybrid Protoneutron Stars with the MIT Bag Model*, Phys. Rev. D **74**, 123001 (2006).

[34] H. Chen, M. Baldo, G. F. Burgio, and H. J. Schulze, *Hybrid Stars with the Dyson-Schwinger Quark Model*, Phys. Rev. D **84**, 105023 (2011).

[35] H. Shen, H. Toki, K. Oyamatsu, and K. Sumiyoshi, *Relativistic Equation of State of Nuclear Matter for Supernova Explosion*, Prog. Theor. Phys. **100**, 1013 (1998).

[36] H. Shen, H. Toki, K. Oyamatsu, and K. Sumiyoshi, *Relativistic Equation of State of Nuclear Matter for Supernova and Neutron Star*, Nucl. Phys. **A637,** 435 (1998).

[37] K. Nakazato, K. Sumiyoshi, and S. Yamada, *Astrophysical Implications of Equation of State for Hadron-Quark Mixed Phase: Compact Stars and Stellar Collapses*, Phys. Rev. D **77,** 103006 (2008).

[38] I. Sagert, T. Fischer, M. Hempel, G. Pagliara, J. Schaffner-Bielich, A. Mezzacappa, F. K. Thielemann, and M. Liebendorfer, *Signals of the QCD Phase Transition in Core-Collapse Supernovae*, Phys. Rev. Lett. **102,** 081101 (2009).

[39] K. Nakazato, K. Sumiyoshi, and S. Yamada, *Stellar Core Collapse with Hadron-Quark Phase Transition*, Astron. Astrophys. **558,** A50 (2013).

[40] T. Fischer, I. Sagert, G. Pagliara, M. Hempel, J. Schaffner-Bielich, T. Rauscher, F. K. Thielemann, R. Kappeli, G. Martinez-Pinedo, and M. Liebendorfer, *Core-Collapse Supernova Explosions Triggered by a Quark-Hadron Phase Transition during the Early Post-Bounce Phase*, Astrophys. J. Suppl. Ser. **194,** 39 (2011).

[41] T. Fischer, N.-U. F. Bastian, M.-R. Wu, P. Baklanov, E. Sorokina, S. Blinnikov, S. Typel, T. Klähn, and D. B. Blaschke, *Quark Deconfinement as a Supernova Explosion Engine for Massive Blue Supergiant Stars*, Nat. Astron. **2,** 980 (2018).

[42] N.-U. F. Bastian, *Phenomenological Quark-Hadron Equations of State with First-Order Phase Transitions for Astrophysical Applications*, Phys. Rev. D **103,** 023001 (2021).

[43] A. Prakash, D. Radice, D. Logoteta, A. Perego, V. Nedora, I. Bombaci, R. Kashyap, S. Bernuzzi, and A. Endrizzi, *Signatures of Deconfined Quark Phases in Binary Neutron Star Mergers*, Phys. Rev. D **104,** 083029 (2021).

[44] D. Logoteta, A. Perego, and I. Bombaci, *Microscopic Equation of State of Hot Nuclear Matter for Numerical Relativity Simulations*, Astron. Astrophys. **646,** A55 (2021).

[45] M. Oertel, M. Hempel, T. Klähn, and S. Typel, *Equations of State for Supernovae and Compact Stars*, Rev. Mod. Phys. **89,** 015007 (2017).

[46] A. R. Raduta, F. Nacu, and M. Oertel, *Equations of State for Hot Neutron Stars*, Eur. Phys. J. A **57,** 329 (2021).

[47] O. DeWolfe, S. S. Gubser, and C. Rosen, *A Holographic Critical Point*, Phys. Rev. D **83,** 086005 (2011).

[48] J. Knaute, R. Yaresko, and B. Kämpfer, *Holographic QCD Phase Diagram with Critical Point from Einstein–Maxwell-Dilaton Dynamics*, Phys. Lett. B **778,** 419 (2018).

[49] R. Critelli, J. Noronha, J. Noronha-Hostler, I. Portillo, C. Ratti, and R. Rougemont, *Critical Point in the Phase Diagram of Primordial Quark-Gluon Matter from Black Hole Physics*, Phys. Rev. D **96,** 096026 (2017).

[50] J. Grefa, J. Noronha, J. Noronha-Hostler, I. Portillo, C. Ratti, and R. Rougemont, *Hot and Dense Quark-Gluon Plasma Thermodynamics from Holographic Black Holes*, Phys. Rev. D **104,** 034002 (2021).

[51] K. Kashiwa, H. Kouno, M. Matsuzaki, and M. Yahiro, *Critical Endpoint in the Polyakov-Loop Extended NJL Model*, Phys. Lett. B **662,** 26 (2008).

[52] B. W. Mintz, R. Stiele, R. O. Ramos, and J. Schaffner-Bielich, *Phase Diagram and Surface Tension in the Three-Flavor Polyakov-Quark-Meson Model*, Phys. Rev. D **87,** 036004 (2013).

[53] R. Stiele and J. Schaffner-Bielich, *Phase Diagram and Nucleation in the Polyakov-Loop-Extended Quark-Meson Truncation of QCD with the Unquenched Polyakov-Loop Potential*, Phys. Rev. D **93,** 094014 (2016).

[54] N. Jokela, M. Järvinen, and J. Remes, *Holographic QCD in the Veneziano Limit and Neutron Stars*, J. High Energy Phys. 03 (2019) 041.

[55] M. Järvinen, *Holographic Modeling of Nuclear Matter and Neutron Stars*, Eur. Phys. J. C **82,** 282 (2022).

[56] U. Gursoy and E. Kiritsis, *Exploring Improved Holographic Theories for QCD: Part I*, J. High Energy Phys. 02 (2008) 032.

[57] U. Gursoy, E. Kiritsis, and F. Nitti, *Exploring Improved Holographic Theories for QCD: Part II*, J. High Energy Phys. 02 (2008) 019.

[58] F. Bigazzi, R. Casero, A. L. Cotrone, E. Kiritsis, and A. Paredes, *Non-Critical Holography and Four-Dimensional CFT's with Fundamentals*, J. High Energy Phys. 10 (2005) 012.

[59] R. Casero, E. Kiritsis, and A. Paredes, *Chiral Symmetry Breaking as Open String Tachyon Condensation*, Nucl. Phys. **B787,** 98 (2007).

[60] G. Veneziano, *Some Aspects of a Unified Approach to Gauge, Dual and Gribov Theories*, Nucl. Phys. **B117,** 519 (1976).

[61] G. Veneziano, *U(1) without Instantons*, Nucl. Phys. **B159,** 213 (1979).

[62] S. S. Gubser, *Curvature Singularities: The Good, the Bad, and the Naked*, Adv. Theor. Math. Phys. **4,** 679 (2000).

[63] T. Alho, M. Järvinen, K. Kajantie, E. Kiritsis, and K. Tuominen, *On Finite-Temperature Holographic QCD in the Veneziano Limit*, J. High Energy Phys. 01 (2013) 093.

[64] T. Alho, M. Järvinen, K. Kajantie, E. Kiritsis, C. Rosen, and K. Tuominen, *A Holographic Model for QCD in the Veneziano Limit at Finite Temperature and Density*, J. High Energy Phys. 04 (**2014**) 124; 02 (2015) 033(E).

[65] U. Gursoy, E. Kiritsis, L. Mazzanti, and F. Nitti, *Deconfinement and Gluon Plasma Dynamics in Improved Holographic QCD*, Phys. Rev. Lett. **101,** 181601 (2008).

[66] U. Gursoy, E. Kiritsis, L. Mazzanti, and F. Nitti, *Holography and Thermodynamics of 5D Dilaton-Gravity*, J. High Energy Phys. 05 (**2009**) 033.

[67] T. Alho, M. Järvinen, K. Kajantie, E. Kiritsis, and K. Tuominen, *Quantum and Stringy Corrections to the Equation of State of Holographic QCD Matter and the Nature of the Chiral Transition*, Phys. Rev. D **91,** 055017 (2015).

[68] M. Panero, *Thermodynamics of the QCD Plasma and the Large-N Limit*, Phys. Rev. Lett. **103,** 232001 (2009).

[69] S. Borsanyi, Z. Fodor, C. Hoelbling, S. D. Katz, S. Krieg, and K. K. Szabo, *Full Result for the QCD Equation of State with $2+1$ Flavors*, Phys. Lett. B **730,** 99 (2014).

[70] S. Borsanyi, Z. Fodor, S. D. Katz, S. Krieg, C. Ratti, and K. Szabo, *Fluctuations of Conserved Charges at Finite Temperature from Lattice QCD*, J. High Energy Phys. 01 (2012) 138.

[71] In principle, working in the Veneziano limit, where $N_f \sim N_c$ should enhance the pressure of the confined matter. However, it turns out that such contributions are not captured only by backreacting the flavor action to the geometry, but one should include nontrivial string loop diagrams [67].

[72] P. A. Zyla *et al.* (Particle Data Group), *Review of Particle Physics*, Prog. Theor. Exp. Phys. **2020**, 083C01 (2020).

[73] D. H. Rischke, M. I. Gorenstein, H. Stoecker, and W. Greiner, *Excluded Volume Effect for the Nuclear Matte Equation of State*, Z. Phys. C **51**, 485 (1991).

[74] R. Hagedorn and J. Rafelski, *Hot Hadronic Matter and Nuclear Collisions*, Phys. Lett. B **97**, 136 (1980).

[75] V. Vovchenko, M. I. Gorenstein, and H. Stoecker, *van der Waals Interactions in Hadron Resonance Gas: From Nuclear Matter to Lattice QCD*, Phys. Rev. Lett. **118**, 182301 (2017).

[76] V. Vovchenko, A. Motornenko, P. Alba, M. I. Gorenstein, L. M. Satarov, and H. Stoecker, *Multicomponent van der Waals Equation of State: Applications in Nuclear and Hadronic Physics*, Phys. Rev. C **96**, 045202 (2017).

[77] V. Vovchenko, D. V. Anchishkin, M. I. Gorenstein, and R. V. Poberezhnyuk, *Scaled Variance, Skewness, and Kurtosis Near the Critical Point of Nuclear Matter*, Phys. Rev. C **92**, 054901 (2015).

[78] K. Redlich and K. Zalewski, *Thermodynamics of van der Waals Fluids with Quantum Statistics*, Acta Phys. Polon. B **47**, 1943 (2016).

[79] H. Toki, D. Hirata, Y. Sugahara, K. Sumiyoshi, and I. Tanihata, *Relativistic Many Body Approach for Unstable Nuclei and Supernova*, Nucl. Phys. **A588**, c357 (1995).

[80] G. Audi, A. Wapstra, and C. Thibault, *The AME2003 Atomic Mass evaluation: (II). Tables, Graphs and References*, Nucl. Phys. **A729**, 337 (2003).

[81] L.-S. Geng, H. Toki, and J. Meng, *Masses, Deformations and Charge Radii: Nuclear Ground-State Properties in the Relativistic Mean Field Model*, Prog. Theor. Phys. **113**, 785 (2005).

[82] M. Hempel, T. Fischer, J. Schaffner-Bielich, and M. Liebendorfer, *New Equations of State in Simulations of Core-Collapse Supernovae*, Astrophys. J. **748**, 70 (2012).

[83] A. W. Steiner, M. Hempel, and T. Fischer, *Core-Collapse Supernova Equations of State Based on Neutron Star Observations*, Astrophys. J. **774**, 17 (2013).

[84] A. Akmal, V. R. Pandharipande, and D. G. Ravenhall, *Equation of State of Nucleon Matter and Neutron Star Structure*, Phys. Rev. C **58**, 1804 (1998).

[85] https://compose.obspm.fr/eos/197.

[86] https://compose.obspm.fr/eos/198.

[87] https://compose.obspm.fr/eos/199.

[88] M. Baldo and G. F. Burgio, *The Nuclear Symmetry Energy*, Prog. Part. Nucl. Phys. **91**, 203 (2016).

[89] We use $T_{\min} = 0.1$ MeV instead of $T = 0$ when evaluating these definitions numerically because this value is the lowest available in the data grid of the HS(DD2) EOS.

[90] F. Karsch, K. Redlich, and A. Tawfik, *Hadron Resonance Mass Spectrum and Lattice QCD Thermodynamics*, Eur. Phys. J. C **29**, 549 (2003).

[91] F. Karsch, K. Redlich, and A. Tawfik, *Thermodynamics at Nonzero Baryon Number Density: A Comparison of Lattice and Hadron Resonance Gas Model Calculations*, Phys. Lett. B **571**, 67 (2003).

[92] M. Albright, J. Kapusta, and C. Young, *Matching Excluded Volume Hadron Resonance Gas Models and Perturbative QCD to Lattice Calculations*, Phys. Rev. C **90**, 024915 (2014).

[93] E. Annala, T. Gorda, A. Kurkela, and A. Vuorinen, *Gravitational-Wave Constraints on the Neutron-Star-Matter Equation of State*, Phys. Rev. Lett. **120**, 172703 (2018).

[94] E. R. Most, L. R. Weih, L. Rezzolla, and J. Schaffner-Bielich, *New Constraints on Radii and Tidal Deformabilities of Neutron Stars from GW170817*, Phys. Rev. Lett. **120**, 261103 (2018).

[95] E. Annala, T. Gorda, A. Kurkela, J. Nättilä, and A. Vuorinen, *Evidence for Quark-Matter Cores in Massive Neutron Stars*, Nat. Phys. **16**, 907 (2020).

[96] E. Annala, T. Gorda, E. Katerini, A. Kurkela, J. Nättilä, V. Paschalidis, and A. Vuorinen, *Multimessenger Constraints for Ultradense Matter*, Phys. Rev. X **12**, 011058 (2022).

[97] O. Komoltsev and A. Kurkela, *How Perturbative QCD Constrains the Equation of State at Neutron-Star Densities*, Phys. Rev. Lett. **128**, 202701 (2022).

[98] B. P. Abbott *et al.* (LIGO Scientific and Virgo Collaborations), *GW170817: Observation of Gravitational Waves from a Binary Neutron Star Inspiral*, Phys. Rev. Lett. **119**, 161101 (2017).

[99] B. P. Abbott *et al.* (LIGO Scientific, Virgo, Fermi GBM, INTEGRAL, IceCube, AstroSat Cadmium Zinc Telluride Imager Team, IPN, Insight-Hxmt, ANTARES, Swift, AGILE Team, 1M2H Team, Dark Energy Camera GW-EM, DES, DLT40, GRAWITA, Fermi-LAT, ATCA, AS-KAP, Las Cumbres Observatory Group, OzGrav, DWF (Deeper Wider Faster Program), AST3, CAASTRO, VINROUGE, MASTER, J-GEM, GROWTH, JAGWAR, CaltechNRAO, TTU-NRAO, NuSTAR, Pan-STARRS, MAXI Team, TZAC Consortium, KU, Nordic Optical Telescope, ePESSTO, GROND, Texas Tech University, SALT Group, TOROS, BOOTES, MWA, CALET, IKI-GW Follow-up, H.E.S.S., LOFAR, LWA, HAWC, Pierre Auger, ALMA, Euro VLBI Team, Pi of Sky, Chandra Team at McGill University, DFN, ATLAS Telescopes, High Time Resolution Universe Survey, RIMAS, RATIR, SKA South Africa/MeerKAT), *Multi-Messenger Observations of a Binary Neutron Star Merger*, Astrophys. J. Lett. **848**, L12 (2017).

[100] L. Rezzolla, E. R. Most, and L. R. Weih, *Using Gravitational-Wave Observations and Quasi-Universal Relations to Constrain the Maximum Mass of Neutron Stars*, Astrophys. J. Lett. **852**, L25 (2018).

[101] M. Drews and W. Weise, *From Asymmetric Nuclear Matter to Neutron Stars: A Functional Renormalization Group Study*, Phys. Rev. C **91**, 035802 (2015).

[102] M. Drews and W. Weise, *Functional Renormalization Group Studies of Nuclear and Neutron Matter*, Prog. Part. Nucl. Phys. **93**, 69 (2017).

[103] K. Otto, M. Oertel, and B.-J. Schaefer, *Hybrid and Quark Star Matter Based on a Nonperturbative Equation of State*, Phys. Rev. D **101**, 103021 (2020).

[104] M. A. Stephanov, *QCD Phase Diagram and the Critical Point*, Prog. Theor. Phys. Suppl. **153,** 139 (2004).

[105] A. Ayala, B. A. Zamora, J. J. Cobos-Martínez, S. Hernández-Ortiz, L. A. Hernández, A. Raya, and M. E. Tejeda-Yeomans, *Collision Energy Dependence of the Critical End Point from Baryon Number Fluctuations in the Linear Sigma Model with Quarks*, Eur. Phys. J. A **58,** 87 (2022).

[106] K. Aryal, C. Constantinou, R. L. S. Farias, and V. Dexheimer, *The Effect of Charge, Isospin, and Strangeness in the QCD Phase Diagram Critical End Point*, Universe **7,** 454 (2021).

[107] C. Yang *et al.* (STAR Collaboration), *The STAR Beam Energy Scan Phase II Physics and Upgrades*, Nucl. Phys. **A967,** 800 (2017).

[108] L. Adamczyk *et al.* (STAR Collaboration), *Bulk Properties of the Medium Produced in Relativistic Heavy-Ion Collisions from the Beam Energy Scan Program*, Phys. Rev. C **96,** 044904 (2017).

[109] X. An *et al.*, *The BEST Framework for the Search for the QCD Critical Point and the Chiral Magnetic Effect*, Nucl. Phys. **A1017,** 122343 (2022).

[110] A. Carbone and A. Schwenk, *Ab Initio Constraints on Thermal Effects of the Nuclear Equation of State*, Phys. Rev. C **100,** 025805 (2019).

[111] A. Bauswein, H. T. Janka, and R. Oechslin, *Testing Approximations of Thermal Effects in Neutron Star Merger Simulations*, Phys. Rev. D **82,** 084043 (2010).

[112] R. De Pietri, A. Feo, J. A. Font, F. Löffler, M. Pasquali, and N. Stergioulas, *Numerical-Relativity Simulations of Long-Lived Remnants of Binary Neutron Star Mergers*, Phys. Rev. D **101,** 064052 (2020).

[113] X. Xie, I. Hawke, A. Passamonti, and N. Andersson, *Instabilities in Neutron-Star Postmerger Remnants*, Phys. Rev. D **102,** 044040 (2020).

[114] A. Figura, J. J. Lu, G. F. Burgio, Z. H. Li, and H. J. Schulze, *Hybrid Equation of State Approach in Binary Neutron-Star Merger Simulations*, Phys. Rev. D **102,** 043006 (2020).

[115] H. T. Cromartie *et al.* (NANOGrav Collaboration), *Relativistic Shapiro Delay Measurements of an Extremely Massive Millisecond Pulsar*, Nat. Astron. **4,** 72 (2020).

[116] E. Fonseca *et al.*, *Refined Mass and Geometric Measurements of the High-Mass PSR J0740 + 6620*, Astrophys. J. Lett. **915,** L12 (2021).

[117] T. E. Riley *et al.*, *A NICER View of PSR J0030 + 0451: Millisecond Pulsar Parameter Estimation*, Astrophys. J. Lett. **887,** L21 (2019).

[118] M. Miller *et al.*, *PSR J0030 + 0451 Mass and Radius from NICER Data and Implications for the Properties of Neutron Star Matter*, Astrophys. J. Lett. **887,** L24 (2019).

[119] M. C. Miller *et al.*, *The Radius of PSR J0740 + 6620 from NICER and XMM-Newton Data*, Astrophys. J. Lett. **918,** L28 (2021).

[120] T. E. Riley *et al.*, *A NICER View of the Massive Pulsar PSR J0740 + 6620 Informed by Radio Timing and XMM-Newton Spectroscopy*, Astrophys. J. Lett. **918,** L27 (2021).

[121] J. Nättilä, M. C. Miller, A. W. Steiner, J. J. E. Kajava, V. F. Suleimanov, and J. Poutanen, *Neutron Star Mass and Radius Measurements from Atmospheric Model fits to X-Ray Burst Cooling Tail Spectra*, Astron. Astrophys. **608,** A31 (2017).

[122] B. P. Abbott *et al.* (LIGO Scientific and Virgo Collaborations), *GW170817: Measurements of Neutron Star Radii and Equation of State*, Phys. Rev. Lett. **121,** 161101 (2018).

[123] M. G. Alford, A. Schmitt, K. Rajagopal, and T. Schäfer, *Color Superconductivity in Dense Quark Matter*, Rev. Mod. Phys. **80,** 1455 (2008).

[124] H.-Y. Chen, K. Hashimoto, and S. Matsuura, *Towards a Holographic Model of Color-Flavor Locking Phase*, J. High Energy Phys. 02 (**2010**) 104.

[125] P. Basu, F. Nogueira, M. Rozali, J. B. Stang, and M. Van Raamsdonk, *Towards A Holographic Model of Color Superconductivity*, New J. Phys. **13,** 055001 (2011).

[126] K. B. Fadafan, J. C. Rojas, and N. Evans, *Holographic Description of Color Superconductivity*, Phys. Rev. D **98,** 066010 (2018).

[127] A. F. Faedo, D. Mateos, C. Pantelidou, and J. Tarrío, *A Supersymmetric Color Superconductor from Holography*, J. High Energy Phys. 05 (2019) 106.

[128] K. Ghoroku, K. Kashiwa, Y. Nakano, M. Tachibana, and F. Toyoda, *Color Superconductivity in a Holographic Model*, Phys. Rev. D **99,** 106011 (2019).

[129] O. Henriksson, C. Hoyos, and N. Jokela, *Novel Color Superconducting Phases of $\mathcal{N} = 4$ Super Yang-Mills at Strong Coupling*, J. High Energy Phys. 09 (2019) 088.

[130] C. Hoyos, M. Järvinen, N. Jokela, J. G. Subils, J. Tarrio, and A. Vuorinen, *Transport in Strongly Coupled Quark Matter*, Phys. Rev. Lett. **125,** 241601 (2020).

[131] C. Hoyos, N. Jokela, M. Järvinen, J. G. Subils, J. Tarrio, and A. Vuorinen, *Holographic Approach to Transport in Dense QCD Matter*, Phys. Rev. D **105,** 066014 (2022).

[132] A. Schmitt and P. Shternin, *Reaction Rates and Transport in Neutron Stars*, Astrophysics and Space Science Library **457,** 455 (2018).

[133] O. Aharony, S. Minwalla, and T. Wiseman, *Plasma-Balls in Large N Gauge Theories and Localized Black Holes*, Classical Quantum Gravity **23,** 2171 (2006).

[134] E. S. Fraga, M. Hippert, and A. Schmitt, *Surface Tension of Dense Matter at the Chiral Phase Transition*, Phys. Rev. D **99,** 014046 (2019).

[135] N. K. Glendenning, *First Order Phase Transitions with More Than One Conserved Charge: Consequences for Neutron Stars*, Phys. Rev. D **46,** 1274 (1992).

[136] C. Hoyos, N. Jokela, D. Rodríguez Fernández, and A. Vuorinen, *Holographic Quark Matter and Neutron Stars*, Phys. Rev. Lett. **117,** 032501 (2016).

[137] E. Annala, C. Ecker, C. Hoyos, N. Jokela, D. Rodríguez Fernández, and A. Vuorinen, *Holographic Compact Stars Meet Gravitational Wave Constraints*, J. High Energy Phys. 12 (2018) 078.

[138] K. B. Fadafan, J. C. Rojas, and N. Evans, *Deconfined, Massive Quark Phase at High Density and Compact Stars: A Holographic Study*, Phys. Rev. D **101,** 126005 (2020).

[139] L. A. H. Mamani, C. V. Flores, and V. T. Zanchin, *Phase Diagram and Compact Stars in a Holographic QCD Model*, Phys. Rev. D **102,** 066006 (2020).

[140] K. B. Fadafan, J. C. Rojas, and N. Evans, *Holographic Quark Matter with Colour Superconductivity and a Stiff*

Equation of State for Compact Stars, Phys. Rev. D **103**, 026012 (2021).

[141] K. Ghoroku, K. Kashiwa, Y. Nakano, M. Tachibana, and F. Toyoda, *Stiff Equation of State for a Holographic Nuclear Matter as Instanton Gas*, Phys. Rev. D **104**, 126002 (2021).

[142] C. Hoyos, N. Jokela, and A. Vuorinen, *Holographic Approach to Compact Stars and Their Binary Mergers*, Prog. Part. Nucl. Phys. **126**, 103972 (2022).

[143] N. Kovensky, A. Poole, and A. Schmitt, *Building a Realistic Neutron Star from Holography*, Phys. Rev. D **105**, 034022 (2022).

[144] A. Bauswein, Niels-Uwe F. Bastian, D. B. Blaschke, K. Chatziioannou, J. A. Clark, T. Fischer, and M. Oertel, *Identifying a First-Order Phase Transition in Neutron Star Mergers through Gravitational Waves*, Phys. Rev. Lett. **122**, 061102 (2019).

[145] P. Möller, J. Nix, and K.-L. Kratz, *Nuclear Properties for Astrophysical and Radioactive-Ion-Beam Applications*, At. Data Nucl. Data Tables **66**, 131 (1997).

[146] F. J. Fattoyev, C. J. Horowitz, J. Piekarewicz, and G. Shen, *Relativistic Effective Interaction for Nuclei, Giant Resonances, and Neutron Stars*, Phys. Rev. C **82**, 055803 (2010).

[147] X. Roca-Maza and J. Piekarewicz, *Impact of the Symmetry Energy on the Outer Crust of Nonaccreting Neutron Stars*, Phys. Rev. C **78**, 025807 (2008).

[148] J. M. Lattimer and F. Douglas Swesty, *A Generalized Equation of State for Hot, Dense Matter*, Nucl. Phys. **A535**, 331 (1991).

[149] M. Oertel, A. F. Fantina, and J. Novak, *Extended Equation of State for Core-Collapse Simulations*, Phys. Rev. C **85**, 055806 (2012).

[150] X. Du, A. W. Steiner, and J. W. Holt, *Hot and Dense Homogeneous Nucleonic Matter Constrained by Observations, Experiment, and Theory*, Phys. Rev. C **99**, 025803 (2019).

[151] X. Du, A. W. Steiner, and J. W. Holt, *Hot and Dense Matter Equation of State Probability Distributions for Astrophysical Simulations*, Phys. Rev. C **105**, 035803 (2022).

[152] N.-U. F. Bastian, *Phenomenological Quark-Hadron Equations of State with First-Order Phase Transitions for Astrophysical Applications*, Phys. Rev. D **103**, 023001 (2021).

[153] https://neutronstars.utk.edu/code/eos/.

[154] K. Hebeler, J. M. Lattimer, C. J. Pethick, and A. Schwenk, *Equation of State and Neutron Star Properties Constrained by Nuclear Physics and Observation*, Astrophys. J. **773**, 11 (2013).

[155] E. S. Fraga, A. Kurkela, and A. Vuorinen, *Interacting Quark Matter Equation of State for Compact Stars*, Astrophys. J. Lett. **781**, L25 (2014).

[156] S. Altiparmak, C. Ecker, and L. Rezzolla, *On the Sound Speed in Neutron Stars*, arXiv:2203.14974.

[157] S. Tootle, C. Ecker, K. Topolski, T. Demircik, M. Järvinen, and L. Rezzolla, *Quark Formation and Phenomenology in Binary Neutron-Star Mergers Using V-QCD*, arXiv:2205.05691.